Computer Assisted Mechanics and Engineering Sciences, **12**: 413–442, 2005.

Numerical simulation of an explosion in a small-scale replica of a Fast Breeder Reactor

Marie-France Robbe
CEA Saclay, Bât 118, 91191 Gif sur Yvette cedex, France
Tel: (33) 1 69 08 87 49, E-mail: marie-france.robbe@cea.fr

Michel Lepareux
CEA Saclay, SEMT-DYN, 91191 Gif sur Yvette cedex, France

Eloi Treille
Socotec Industrie, 1 av. du Parc, 78180 Montigny le Bretonneux, France

Yves Cariou
Novatome, NVPM, 10 rue Juliette Récamier, 69006 Lyon, France

(Received October 7. 2005)

A Core Disruptive Accident in a Liquid Metal Fast Breeder Reactor (LMFBR) results from the interaction between molten fuel and liquid sodium, which creates a high-pressure bubble of gas in the core. The violent expansion of this bubble loads and deforms the vessel and the internal structures. The MARS experimental test simulates a hypothetical Core Disruptive Accident in a small-scale mock-up containing all the significant internal components of a LMFBR. This paper presents a numerical simulation of the test with the EUROPLEXUS code.

1. Introduction

In case of a Hypothetical Core Disruptive Accident (HCDA) in a Liquid Metal Fast Breeder Reactor (LMFBR), the interaction between the molten fuel and the liquid sodium creates a high-pressure gas bubble in the core. The violent expansion of this bubble loads and deforms the vessel and the internal structures.

During the 1970s and 1980s, the LMFBR integrity was studied with codes especially devoted to the analysis of transient loads resulting from a HCDA: PISCES 2 DELK [16], REXCO [12], MICE, ICECO, ICEPEL, STRAW and SADCAT [13], SURBOUM [57], SEURBNUK/EURDYN [7, 54, 56], ASTARTE [15], CASSIOPEE [21], SIRIUS [1, 4, 17], etc.

In order to validate these codes, experimental programmes and benchmarks were undertaken by several countries: COVA [2, 23, 24, 26, 59], APRICOT [60], WINCON [53], STROVA [27], CONT [3], MARA for instance.

The French experimental programme MARA [5, 34] was based on scale models of the Superphenix reactor, and involved eleven tests of gradual complexity due to the addition of internal deformable structures:

- MARA 1 and 2 considered a flexible vessel partially filled with water and closed by a rigid roof [1],
- MARA 4 represented the main core support structures [55],

- MARA 8 and 9 were closed by a flexible roof [20],
- MARA 10 included the core support structures and a simplified representation of the structures above the core [33],
- MARS [19] was a 1/20-scale mock-up including all the significant internal components.

Nowadays, the computer codes developed and used in the 1970s and 1980s are no longer used. In France, a specific HCDA sodium-bubble-argon tri-component constitutive law [30] was added to the general ALE fast dynamics finite element CASTEM-PLEXUS code at the end of the 1980s. The HCDA constitutive law was qualified [11] on the CONT benchmark.

At the beginning of the 1990s, axisymmetrical computations of the MARA series were confronted with the experimental results [8, 9, 31]. The computations showed a rather good agreement with the experimental results for the MARA 8 and MARA 10 tests even if there were some discrepancies. On the contrary, the prediction of the MARS structure displacements and strains was overestimated [10].

In 1999, the CASTEM-PLEXUS code was merged with the PLEXIS-3C code [6] (a former joint product by CEA and JRC) to extend the capacities of both codes. The new-born EUROPLEXUS code benefitted from a new method to deal with the fluid-structure coupling and further comparisons between experimental and numerical results were undertaken for the MARA 8 mock-up [41, 45], the MARA 10 mock-up [46, 51] and the MARS test [38, 39, 47, 52] using, in addition, a finer size of the mesh.

In this simulation of the MARS test, the top closure is represented by massive structures, the main internal structures are described by shells, while the peripheral massive structures are taken into account with a pressure loss because their geometry is too complicated to mesh them. The computation uses the new process of fluid-structure treatment. After a brief presentation of the MARS mock-up, the paper focuses on the analysis of the numerical results.

2. Description of the MARS mock-up

The primary circuit of the Superphenix reactor (Fig. 1) is a "pool" design [35]. The whole core, primary pumps and intermediate heat exchangers are enclosed in the main reactor vessel which is made of stainless steel and welded to the roof slab. The main reactor vessel is encased in a safety vessel also made of stainless steel.

The MARS test (Fig. 2) was performed at the CEA-Cadarache in order to simulate a Hypothetical Core Disruptive Accident in a 1/20-scale mock-up of the Superphenix reactor block. The mock-up includes a main vessel, two inner vessels and all the significant internal components of the reactor [19].

The main vessel is 1 m in diameter, 1 m high and of variable thickness (0.8 to 1.6 mm). It is composed of an assembly of a cylindrical part made of 316L stainless steel and a torospherical bottom made of 304L stainless steel. The two inner vessels are completed by the anti-convecting device and the main vessel cooling system.

The core cover plug is a rather complicated structure, despite simplifications compared with the reactor geometry: the mock-up includes the top plate, the in-pile shell with its pipes, the spacer plates and the heat-insulation. The core catcher is composed of the catcher plate, support structure, vertical flanges, chimney and spacing feet.

The lateral neutron shielding is represented by four radially split shells and their supporting structures. The mass of the unmelted part of the core is simulated by a mixing of aluminium cylinders and steel hexagons fixed into two AG3 aluminium plates. The strongback and the diagrid support are respectively represented by a non-axisymmetrical ring and a cylinder.

The roof slab is constituted by two circular plates of different thicknesses to simulate the real reactor roof stiffness. Openings were drilled to enable the passage of the large components and the two rotating plugs are concentrically off as in the reactor.

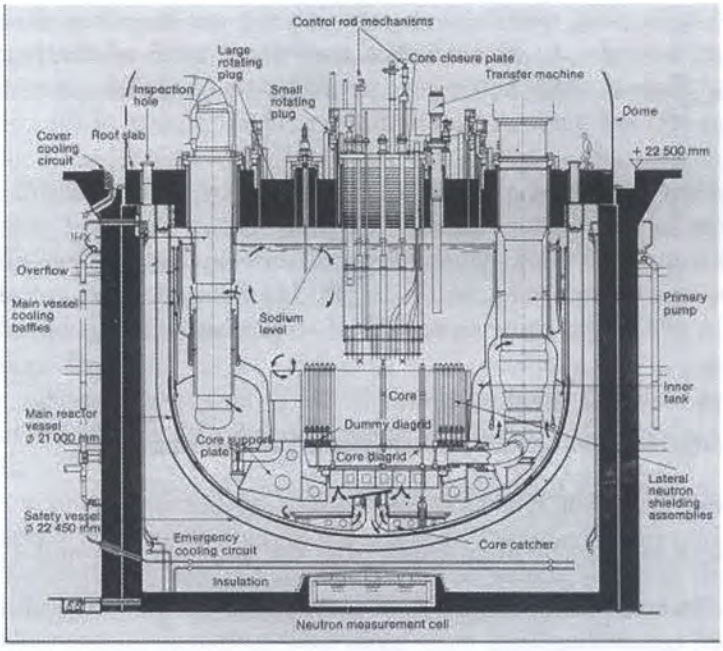

Fig. 1. The Superphenix reactor

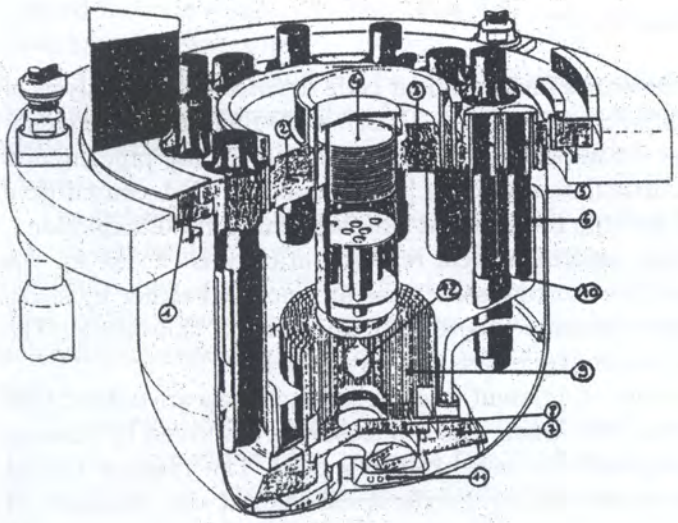

mark 1: roof
mark 2: large rotating plug
mark 3: small rotating plug
mark 4: core cover plug
mark 5: main vessel
mark 6: internal vessels
mark 7: core support structures
mark 8: diagrid support
mark 9: core and neutron shieldings
mark 10: pumps and heat exchangers
mark 11: core catcher

Fig. 2. The MARS mock-up

The main components inserted through the roof slab are modelled: four primary pumps, eight intermediate heat exchangers, four emergency cooling exchangers and two integrated purification devices. The various supporting rings (roof slab, core support structure, large components) and joining rings (between the roof slab and the rotating plugs) are also represented.

The mass deficit of the mock-up cover simulation is compensated by lead plates providing additional weights on the cover. The safety vessel, the dome, the biological shield plates and the handling machine are represented only by their inertia using lead plates. Rubber-ring bands simulate the heat-insulating material between the roof and the main vessel, and the gas intervals of the roof slab.

The thin structures (inner vessels, baffles, lateral neutron shielding, main components, emergency heat exchangers, core cover plug, core catcher, core, joining and supporting rings) are mainly made of 304L stainless steel in order to simulate the austenistic steel of the reactor structures. The massive structures and those made of heterogeneous materials (roof slab, rotating plugs, core support structure, diagrid support) are made of A5 aluminium. The top plate of the core cover plug is made of A42 aluminium.

The sodium coolant at operating conditions is simulated by water at 20°C. The cover gas of the mock-up is the same as in the reactor (argon).

The test was fired using a 80 g low-density low-pressure explosive charge of L54/16 composition [18]. The charge mass was chosen to simulate the 800 MJ full-scale mechanical energy release used in the reference HCDA of the Superphenix reactor. The explosive charge was supported by the base of the core cover plug.

The whole test was well instrumented with:

- 19 pressure transducers fitted on the roof slab and the rotating plugs,
- 5 accelerometers placed on the reactor cover,
- 24 strain gauges attached on the main vessel, roof slab support ring and cover joining rings,
- 3 high-speed cameras used to record the displacements of the main vessel, roof slab, large plug, small plug and core cover plug,
- residual deformations were evaluated by measuring, before and after the firing, the mesh sizes of the grid drawn on the different structures.

3. Numerical modeling of the mock-up

EUROPLEXUS [14, 22, 36] is a general fast dynamics finite element code devoted to the analysis of problems involving fast transients. EUROPLEXUS can perform 1D, 2D or 3D fluid-structure calculations as required. The main fields dealt with are impacts [37], explosions [40, 42, 48], pipe circuits [28, 29, 43, 49, 50], hydrodynamics [58] and articulated systems [32]. A specific CDA constitutive law was implemented in the code in order to be able to represent precisely this kind of explosion.

Owing to the symmetry of the mock-up, an axisymmetrical representation was chosen for the numerical simulation of the MARS mock-up. The external structures are modeled either by shells or massive structures. The main internal structures are described with classical thin shells. The peripheral structures are globally taken into account by means of a pressure loss.

The main vessel is described by three thin shells of different thicknesses; materials are different for the cylindrical part and the torospherical part of the vessel. The top closure is described by massive elements for the roof, the small rotating plug and the large rotating plug. The massive fixings hanging the mock-up to the rigid frame are represented by a cylindrical shell at the extremity of the roof.

The top closure is assimilated to an axisymmetrical structure for the needs of the numerical simulation. The openings in the roof for the passage of the components (pumps, heat exchangers) are simply accounted for by the mass they remove to the roof.

Local masses are added on the top of the roof and the rotating plugs to consider the mass of the instrumentation and the lead plates compensating the deficit of mass of the MARS mock-up compared to the real reactor. The local mass at the centre of the roof also includes the weight of the internal components (pumps, heat exchangers, purification devices). The local mass at the edge of the roof simulates the lead plates used in the mock-up to describe the inertia of the safety vessel, the dome, the biological shield plates and the handling machine.

The core cover plug was simplified. The upper part is modeled by a top plate, the heat and neutronic insulation by three plates. The pipes are assimilated to two vertical cylinders. The in-pile shell, the three spacer plates, and the external shell surrounding the plug are also meshed.

The joining rings between the roof slab and the three plugs are formed, in the mock-up, by cylindrical plates linked by a bridle at their top extremity. They are modeled by thin shells, made of aluminium, joining the top of the massive structures. Complementary shell elements made of rubber and joining the base of the massive structures were added to prevent the going up of argon by the free slits.

The heat-insulating material between the roof and the main vessel is represented by an horizontal rubber-ring band joining the roof base to the main vessel and preventing the upwards motion of argon in the empty slit. The main vessel, hung to the roof in the MARS mock-up, is fixed rigidly to the roof in the numerical model.

In the centre of the mock-up, the strongback, the neutron shielding support, the support of the baffles and of the internal vessel being fitted together, they are modeled by a single rigid structure called the Core Support Structure (CSS). This structure is assimilated to an axisymmetrical shell of constant thickness, whose mass is that of all the structures. The CSS is supposed to be rigid and to transmit the totality of the forces to the structures fixed on it. The CSS is attached to the vessel by a cylindrical collar.

The diagrid support is represented by a thin shell. The core is not meshed: it is simply taken into account by an added mass spread along the diagrid. The diagrid support is fixed to the Core Support Structure by a swivel link. Only the central shell, among the four shells schematizing the neutron shielding in the MARS mock-up, is meshed. This shell governs the fluid port between the core cover plug and the neutron shielding. The three other shells are taken into account by a local mass added at the base of the central neutron shielding shell.

The baffles surrounding the outer neutron shielding are assimilated to an axisymmetrical structure and represented by a vertical shell. The internal vessel is composed of two shells. Only the central one is meshed; the second one is simply described by a local mass added at the base of the meshed internal vessel. The shielding, the baffle shell, and the internal vessel are embedded in the Core Support Structure.

The core catcher could not be meshed because its complex geometry would impose a lot of shells of small dimensions and therefore a very fine local meshing, not compatible with the rest of the model. Consequently, it is represented by an added mass spreaded along the bottom of the main vessel.

The behaviour of the structures previously quoted is generally described with isotropic elastic-plastic constitutive laws. However elastic laws are used to describe the rubber elements of weak resistance joining the different parts of the roof and the plugs. The two cylinders schematizing the pipes of the core cover plug are described by an elastic law approximated by homogenizing the non-axisymmetrical structures. The behaviour of the Core Support Structure is supposed linear elastic.

The internal components (pumps and heat exchangers) are taken into account in a global way. They are represented by a pressure loss applied along a cylinder located at the average radius of the components. The pressure loss coefficient is estimated from [25], supposing that a cylindrical obstacle partially blocks up the port. The surface of this obstacle is given by the ratio between the solid section and the total section for a 1 radian angle.

Figures 3 and 4 present the complete mesh of the MARS test and the structure representation.

In case of a Core Disruptive Accident, the internal fluids are sodium, argon and a gas bubble. In the MARS test, the sodium and bubble are replaced by water and an explosive charge, respectively. Water and argon are initially at the atmospheric pressure whereas the explosive charge induces an initial pressure of 288 MPa in the bubble area.

The characteristics taken into the numerical model are:

• Water	: $\rho = 998.3\,\mathrm{kg/m^3}$	sound speed $C = 1550\,\mathrm{m/s}$	$p^{(0)} = 10^5\,\mathrm{Pa}$
• Argon	: $\rho = 1.658\,\mathrm{kg/m^3}$	heat ratio $\lambda = c_p/c_v = 1.67$	$p^{(0)} = 10^5\,\mathrm{Pa}$
• Explosive charge	: $\rho = 400\,\mathrm{kg/m^3}$	polytropic coef. $\eta = 1.322$	$p^{(0)} = 2.88\ 10^8\,\mathrm{Pa}$
		heat ratio $\lambda = 1.24$	

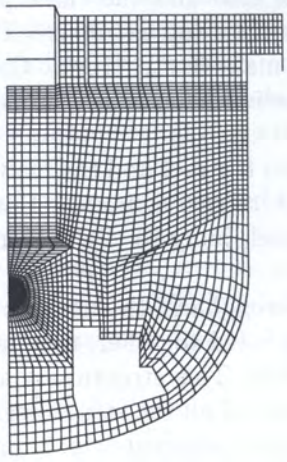

Fig. 3. Mesh of the MARS test

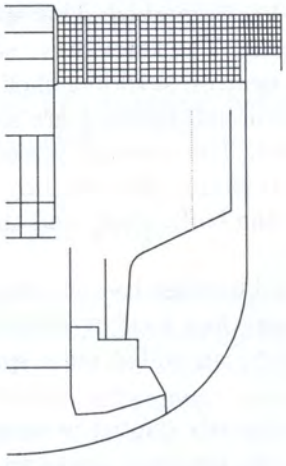

Fig. 4. Mesh of the structures

In the EUROPLEXUS simulation, structures are represented with a Lagrangian description, the bubble zone is kept fixed, water and argon are described with an ALE modeling. Two kinds of fluid-structure coupling are available in EUROPLEXUS [41, 45, 46].

The FSA coupling was adopted for the MARS test because the presence of the internal structures involved large local displacements of the fluid grid. In the previous CASTEM-PLEXUS computations [10], the FS2D coupling was used because the FSA coupling was developed later. However, in the current model, a FS2D coupling persists in a local area.

As the diagrid is merely put down on the Core Support Structure and as both structures are not rigidly linked, the diagrid extremity is linked to the CSS by a swivel contact. Consequently, there are two different structure nodes at the same location (the one pertaining to the diagrid and the other to the CSS) whereas there is only one fluid node facing the two structure ones. This configuration cannot be processed by the FSA coupling. Therefore a FS2D coupling was settled down at the connection between the diagrid, the Core Support Structure and the fluid between the radial shielding and the CSS.

The boundary conditions are:

- Complete blocking of the base of the fixing shell hanging the mock-up to the rigid frame.

- No rotation of all the nodes of the top closure at the intersection between the massive structures and the shells: links between the joining rings, the roof slab and the small and large rotating plugs, link between the roof and the top of the main vessel, links at the extremities of the heat-insulating material between the roof and the main vessel, link between the roof edge and the fixing shell.
- No horizontal displacement and no rotation of the structure nodes located on the symmetry axis (core cover plug, diagrid, vessel), and the nodes of the plates simulating the heat and neutronic insulation of the core cover plug.
- No horizontal displacement of the fluid nodes on the symmetry axis.
- No horizontal displacement of the Core Support Structure.
- Vertical displacement of the CSS equal to the displacement of the point at the intersection between the collar and the vessel.
- Same vertical displacement for the four plates simulating the heat and neutronic insulation of the core cover plug.

To link a shell to a massive structure, it is necessary to impose identical displacements to the nodes facing each other, at the shell extremity and in the massive structure. Are concerned the diagrid and the CSS, the roof and the fixing shell, the roof and the main vessel, the joining rings of the top closure.

In order to help the code to calculate correctly the ALE mesh update in the areas of high fluid speed or high pressure variations, the user has to define relations governing the local displacement of the mesh. Three governing lines were set up.

The first line imposes to the fluid nodes between the lower plate of the core cover plug and the top of the neutron shielding to stay aligned between both structure nodes during the displacement of the structures. This relation prevents a large deformation of the ALE grid due to the huge flow of the fluid going out from the central zone. Besides, this line is used as a reference for the update of the fluid in the central zone.

Two lines keep aligned the fluid nodes between the top of the lateral shielding and the baffle and between the baffle and the internal vessel. These lines prevent a distortion of the fluid mesh due to the large local motions of the structures in this area.

Inside the core cover plug, no fluid-structure coupling is defined because the fluid can cross the pipes simulated by vertical cylinders, and the upper part of the external perforated shell surrounding the plug. Consequently, in order to preserve a regular meshing inside the core cover plug, the fluid nodes on the vertical lines between the lower plate simulating the heat and neutronic insulation and the upper spacer plate have to stay aligned between the structure nodes of both plates.

4. Analysis of the results

The results are described through the evolution of several variables versus time: pressure, presence fraction of gas, fluid speed, deformed shape of the mesh and structures, radial and vertical displacements of structures, stresses and strains in structures.

4.1. Pressure

Figure 5 presents the evolution of pressure versus time in the whole mock-up. Initially, water and argon are at the atmospheric pressure whereas the explosive charge simulating the bubble of gas is at 288 MPa. From 0.02 ms, a pressure wave issued from the bubble zone expands spherically.

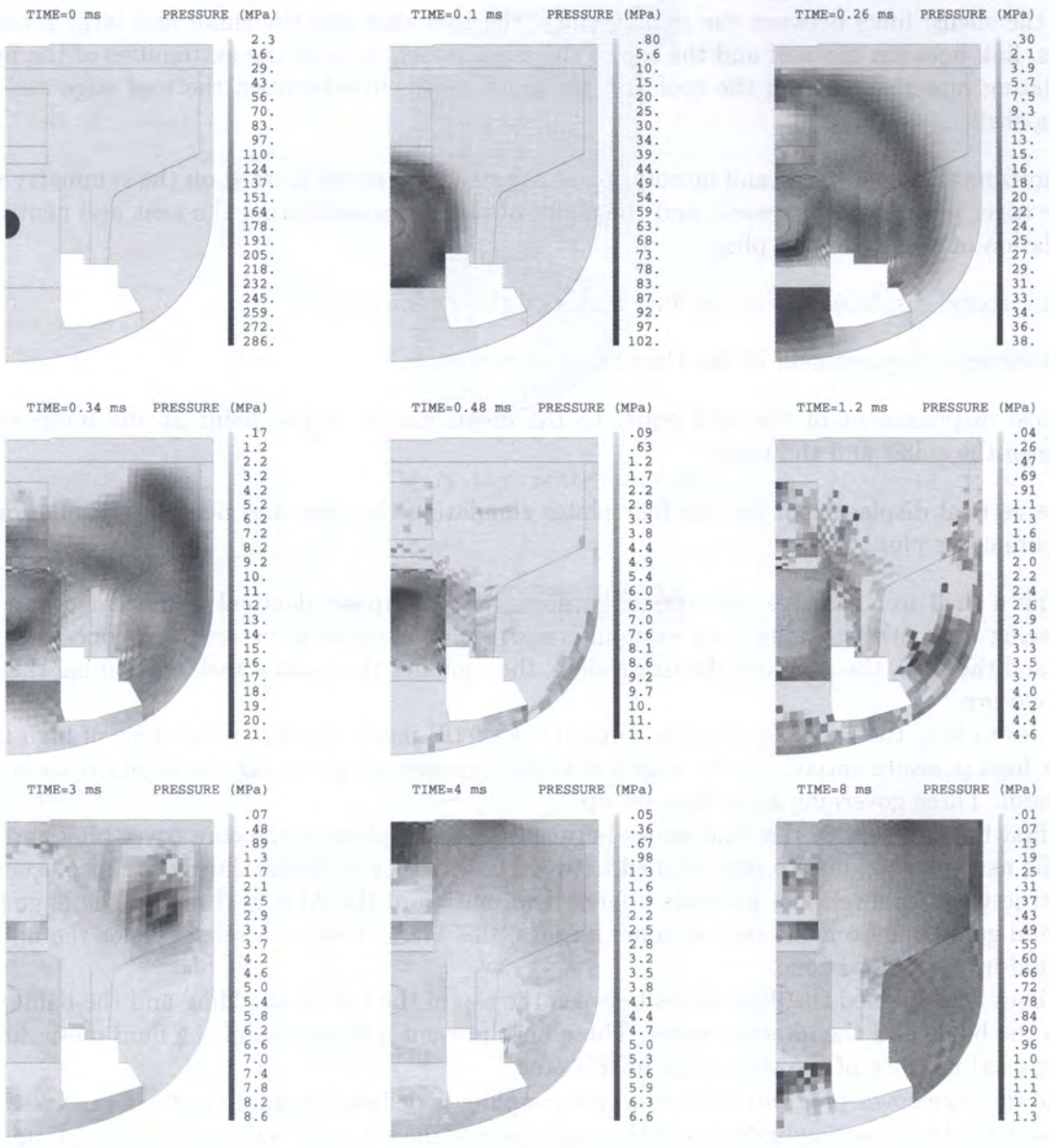

Fig. 5. Pressure (MPa)

At 0.06 ms, the pressure wave hits the nearest structures: the lateral shielding, the in-pile shell of the Core Cover Plug (CCP) and the diagrid. At 0.1 ms, pressure has fallen down to 60 MPa. The pressure wave has crossed the shielding and the in-pile shell, so that it impacts the baffle and the second spacer plate of the CCP. The downward propagation of the pressure wave is temporarily stopped by the diagrid.

At 0.14 ms, the pressure wave succeeds in accelerating the water below the diagrid but pressure is limited to 12 MPa. In the upper part, the pressure wave continues its spherical propagation and impacts the lower part of the internal vessel.

At 0.18 ms, the pressure wave hits the upper spacer plate of the CCP. Pressure is higher at the bottom of the central zone due to the confinement of structures. A small depressurisation appears in the centre of the bubble, and between the in-pile shell and the lower spacer plate.

The pressure wave keeps a spherical shape until 0.22 ms. Then the wave progresses laterally because the vertical expansion is prevented by the presence of the main vessel at the bottom and

the argon layer at the top. At 0.26 ms, the pressure wave impacts the bottom of the main vessel, while depressurised zones appear at the bottom of the central zone (previously the most pressurised water area) and in the middle of the CCP.

At 0.3 ms, the pressure wave has completely gone round the CSS and hits the top of the torospherical part of the main vessel. The maximum pressures are equal to 25 MPa below the diagrid and 18 MPa at the level of the internal vessel. The depressurised areas at the bottom of the central zone and the top of the CCP extend while a new depressurised area forms between the lateral shielding and the baffle. The argon layer always remains at a low pressure because of the compressibility of the gas.

At 0.34 ms, the pressure wave continues its lateral progression and hits the cylindrical part of the main vessel. From 0.38 ms, the average pressure is much lower in the whole mock-up. The maximum pressure reaches only 12 MPa in the central zone and against the top of the internal vessel. Indeed the lateral development of the pressure wave leads to a sort of queue which impacts the intermediate and upper parts of the internal vessel.

From 0.42 to 0.8 ms, the maximum pressure is limited to 10 MPa. Globally, the pressurised areas are concentrated in the central zone, between the radial shielding and the internal vessel, in the CCP and against the main vessel.

Between 1.2 and 2.4 ms, pressure decreases in the entire mock-up. At about 3 ms, a pressure increase appears against the upper part of the internal vessel due to a concentration of fluid in this area. The pressure evolution is no longer governed by acoustic phenomena but hydraulic ones.

4.2. Gas fraction

Figures 6 to 8 show respectively the general volume presence fraction of gas, the mass presence fractions of the bubble and the argon. Initially, the mock-up is filled with water except in the centre where the explosive charge is located and below the top closure which shelters the argon layer.

Between 0.02 and 0.2 ms, the bubble of gas grows spherically and remains confined in the central area due to the presence of the diagrid support, the lateral neutron shielding and the in-pile plate of the core cover plug. At 0.2 ms, the argon layer starts being compressed upwards in the CCP and below the small rotating plug because of the arrival of the pressure wave impacting the top closure.

From 0.4 ms, water vaporises in the areas that became depressurised after the passing of the pressure wave. For instance, at the bottom of the central area and at the top of the CCP, water vaporises since pressure has decreased down to the atmospheric pressure.

Between 0.8 and 2 ms, steam appears in large areas of the mock-up: below and above the diagrid, under the top closure, around the internal vessel, above the upper spacer plate in the CCP and along the vertical structures (the lateral shielding, the baffle and the lower part of the internal vessel). All these areas are at a low pressure when water vaporises.

But, as soon as pressure increases again, steam condenses. For example, below the internal vessel, water vaporises at the atmospheric pressure between 0.8 and 1.2 ms; then steam condenses after 1.6 ms because pressure has locally increased.

Meanwhile, the pressurised bubble of gas goes on expanding in the central area. At 1.2 ms, the bubble is shifted upwards. From 1.6 ms, it starts flowing out of the central zone by the free channel between the top of the neutron shielding and the base of the CCP. The bottom of the central area is filled with liquid water, trapped there by the confinement of structures and the growth of the bubble.

The argon layer is progressively compressed upwards against the top closure between 0.2 and 1 ms. From 1.6 to 4 ms, it is pushed sideways and concentrated in the top right-hand corner, near the junction of the roof and the main vessel, due to the thrust of the water ejected from the central area.

Between 3 and 10 ms, the bubble gas expands out of the central zone. A large panache forms between the external cylinder surrounding the CCP and the internal vessel. Simultaneously, steam

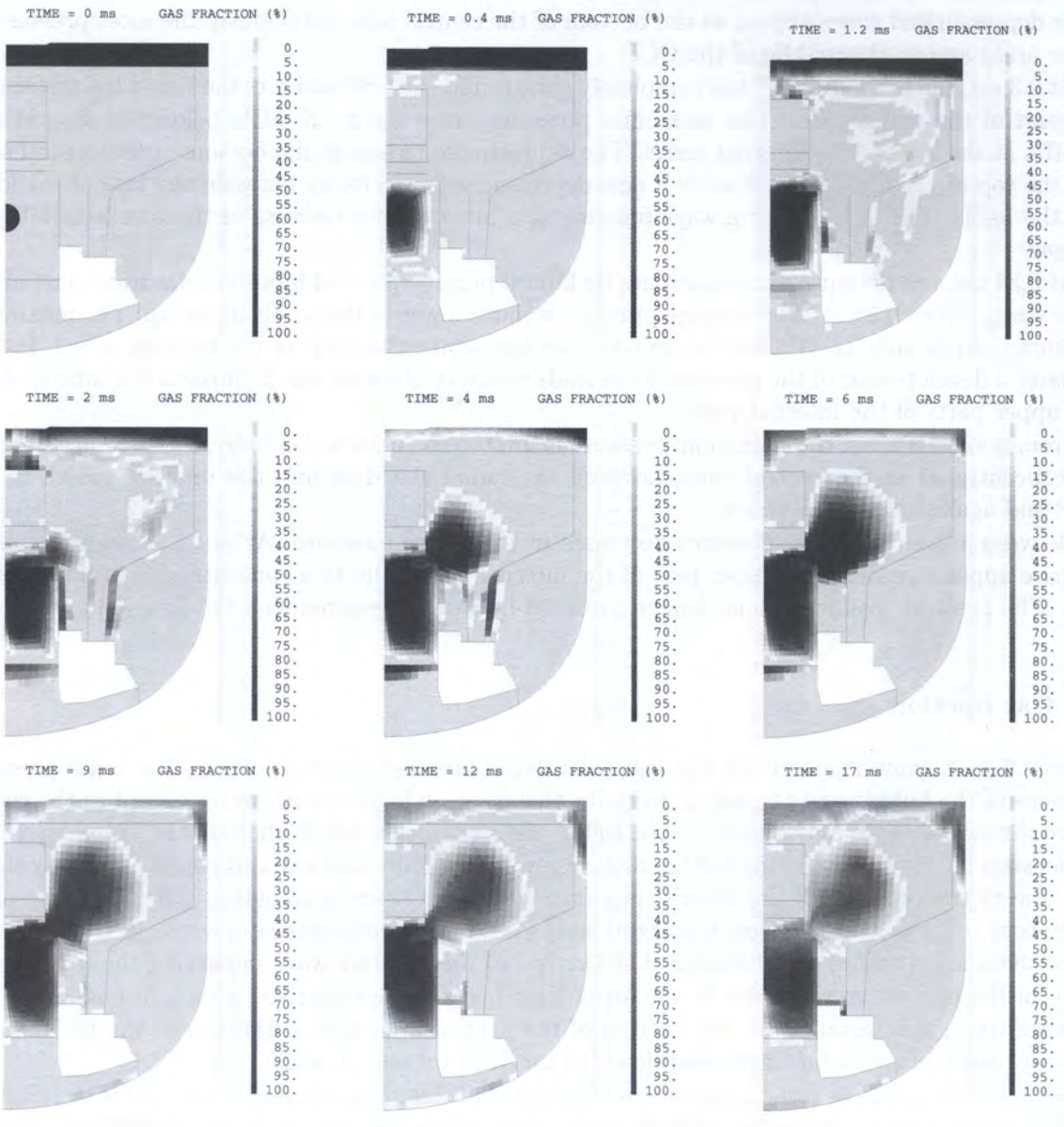

Fig. 6. Volume presence fraction of gas

condenses in the vicinity of the neutron shielding, the baffle and the internal vessel because the expansion of the bubble gas causes a pressure raise in these areas.

On the contrary, water vaporises below the diagrid because water flows down towards the main vessel, the area empties from fluid and consequently pressure decreases. From 5 ms, argon expands along the top closure and the upper part of the main vessel due to the general pressure decrease in the mock-up.

From 10 ms, the bubble gas stops expanding out of the central area due to the formation of a fluid whirlpool between the core cover plug and the internal vessel. Water vaporises between the neutron shielding and the baffle because the whirlpool sucks up water from the periphery.

The bubble is pushed back in the central area and expands downwards in this confined zone. The bubble fills almost completely the central area at 17 ms, so that the trapped water is concentrated at the bottom along the diagrid and the symmetry axis. From 14 ms, the bubble gas above the neutron shielding moves slightly away from the central structures and forms a sort of bag that twirls round in the middle of water.

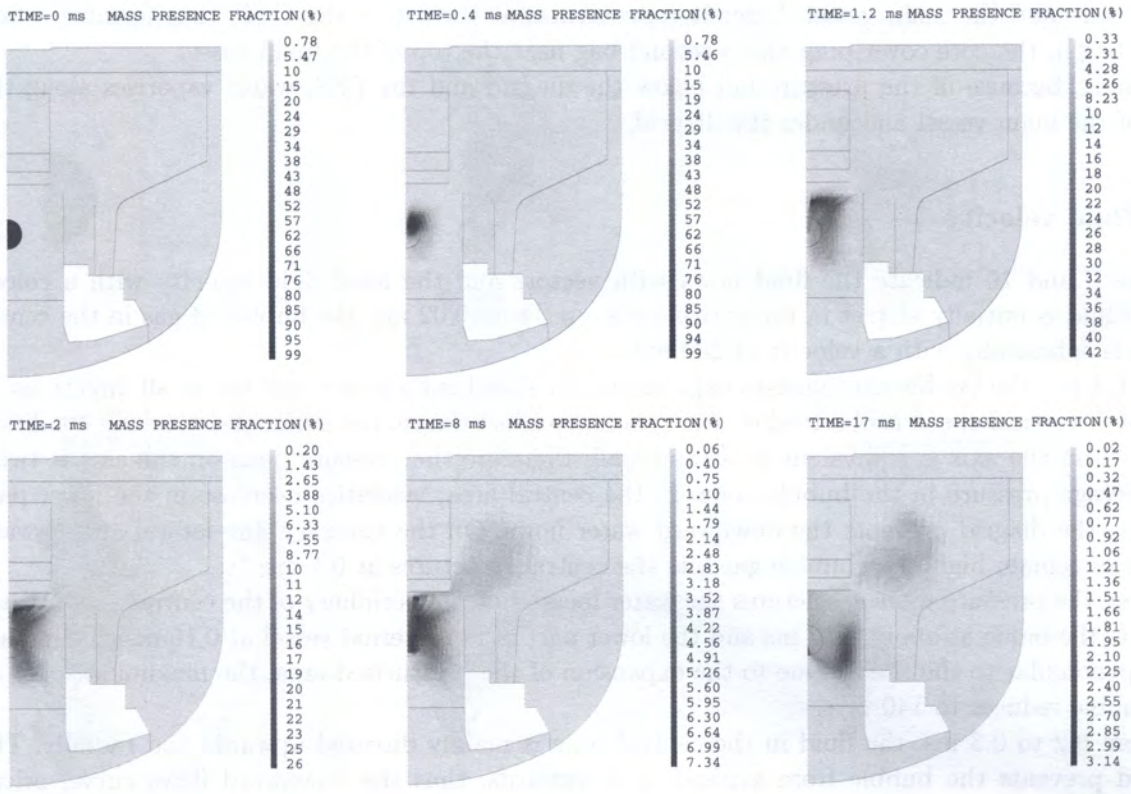

Fig. 7. Mass presence fraction of the bubble

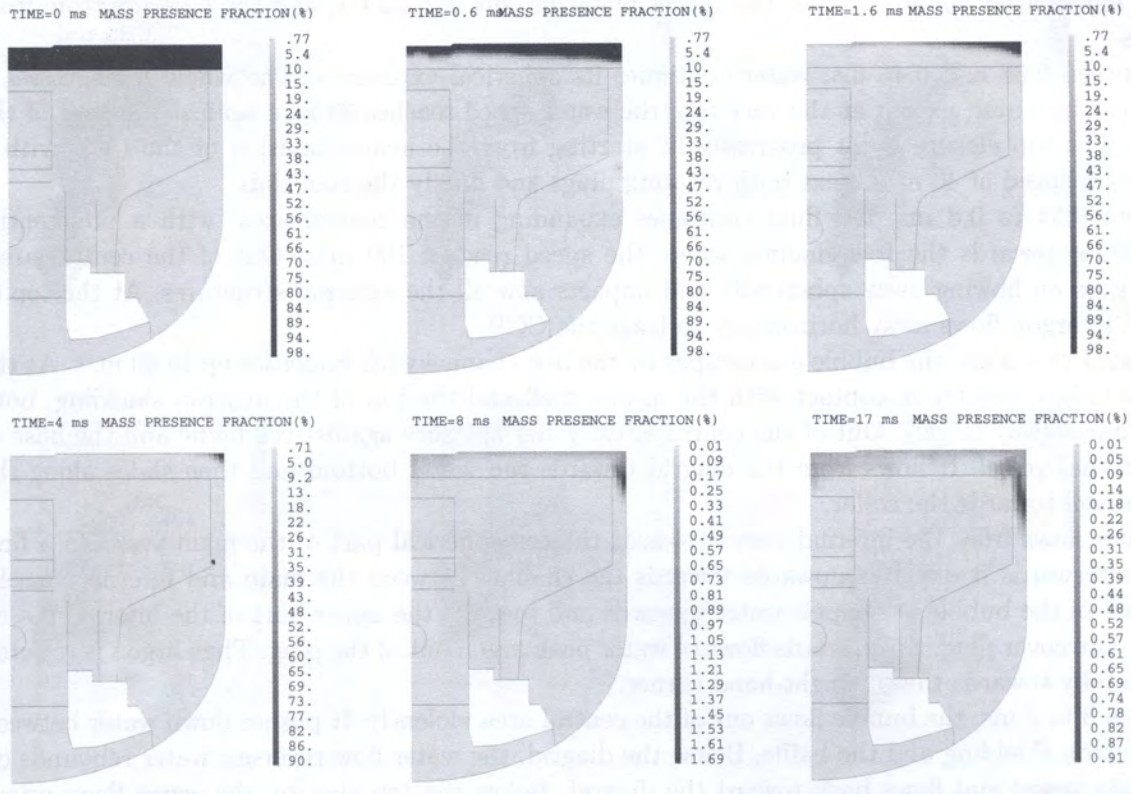

Fig. 8. Mass presence fraction of argon

Argon continues expanding from the top right-hand corner toward the symmetry axis along the top closure and the main vessel. Later it concentrates at the top of the CCP, thus forming a first argon bag in the core cover plug and a second bag near the top of the main vessel.

Finally, because of the pressure fall below the diagrid and the CSS, water vaporises along the base of the main vessel and under the diagrid.

4.3. Fluid velocity

Figures 9 and 10 indicate the fluid flows with vectors and the local fluid velocity with a colour map. Fluid is initially at rest in the entire mock-up. From 0.02 ms, the bubble of gas in the centre expands spherically with a velocity of 200 m/s.

At 0.1 ms, the bubble continues to expand but the speed is no longer uniform in all directions. A very high vertical speed is observed on the symmetry axis because the horizontal blocking condition imposed on the axis is equivalent to a rigid wall; therefore the pressure peak on the axis is twice the average pressure in the bubble zone. In the central area, velocities decrease in the lower part because the diagrid prevents the downward water flows. On the contrary, the lateral and upward velocities remain high. The bubble gas hits the central structures at 0.1 ms.

Then the pressure wave accelerates the water located at the periphery of the central zone. Water impacts the baffle at about 0.12 ms and the lower part of the internal vessel at 0.16 ms; the impact is perpendicular to the shells. Due to the expansion of the pressurised area, the maximum speed of the bubble reduces to 140 m/s.

From 0.2 to 0.3 ms, the fluid in the central zone is mainly directed upwards and radially. The diagrid prevents the bubble from expanding downwards, thus the downward flows curve, orient outwards and hit the neutron shielding with speeds up to 80 m/s. The central fluid thrust pushes the in-pile plate of the CCP upwards and the neutron shielding radially. In the rest of the mock-up, water moves away spherically. All the spacer plates are hit at 0.22 ms, and the vessel bottom from 0.3 ms.

Between 0.38 and 0.46 ms, water continues its spherical expansion. The whole main vessel is impacted by water, except at the very top; the water speed reaches 30 m/s against the base of the vessel. The top closure is hit progressively, starting from the heat-insulation of the CCP with a maximum speed of 40 m/s, next both rotating plugs and finally the roof slab.

From 0.54 to 0.8 ms, the fluid continues expanding in the central area, with a preferential orientation towards the free channel where the speed reaches 100 m/s. Out of the central area, water goes on flowing away spherically and impacts now all the external structures. At the top of the CCP, argon flows away horizontally to leave the CCP.

From 1 to 2.5 ms, the bubble gas escapes by the free channel with velocities up to 90 m/s. As the bubble enters directly in contact with the in-pile shell and the top of the neutron shielding, both shells move away largely. Out of the central area, water splashes against the baffle and the base of the internal vessel. It flows from the diagrid towards the vessel bottom and then slides along the main vessel towards the collar.

Water flows from the internal vessel towards the torospherical part of the main vessel in a first time; afterwards it deviates upwards towards the channel between the main and internal vessels. The exit of the bubble gas expels water upwards and towards the upper part of the internal vessel. In the core cover plug, the upwards flows of water push argon out of the plug. Then argon is rejected horizontally towards the top right-hand corner.

From 3 to 5 ms, the bubble flows out of the central area violently. It pushes down water between the neutron shielding and the baffle. Below the diagrid, the water flow reverses: water rebounds on the main vessel and flows back toward the diagrid. Below the top closure, the water flows orient progressively towards the top right-hand corner. The high horizontal speeds of about 80 m/s just under the top closure are due to outwards argon flows.

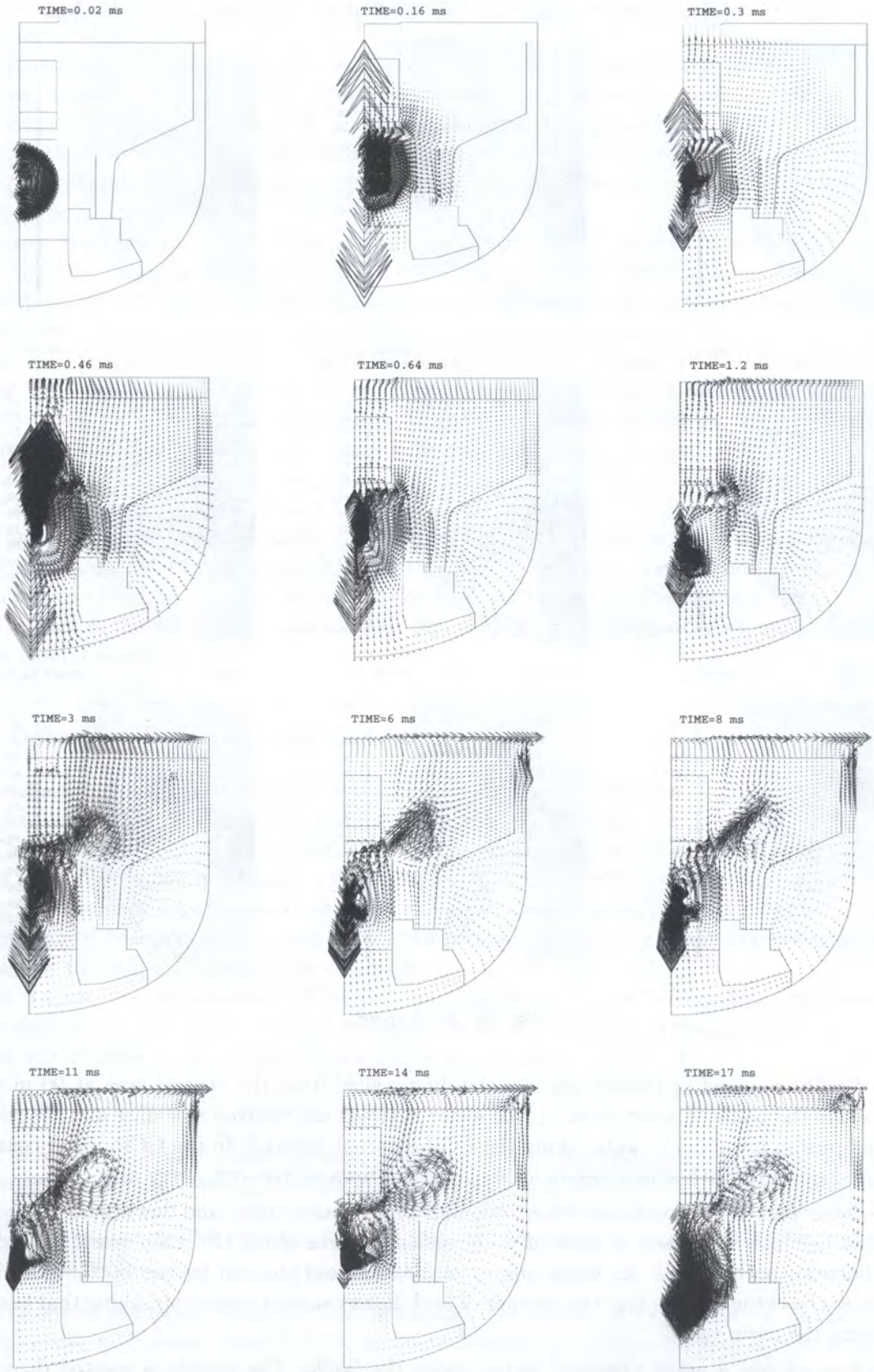

Fig. 9. Fluid flows

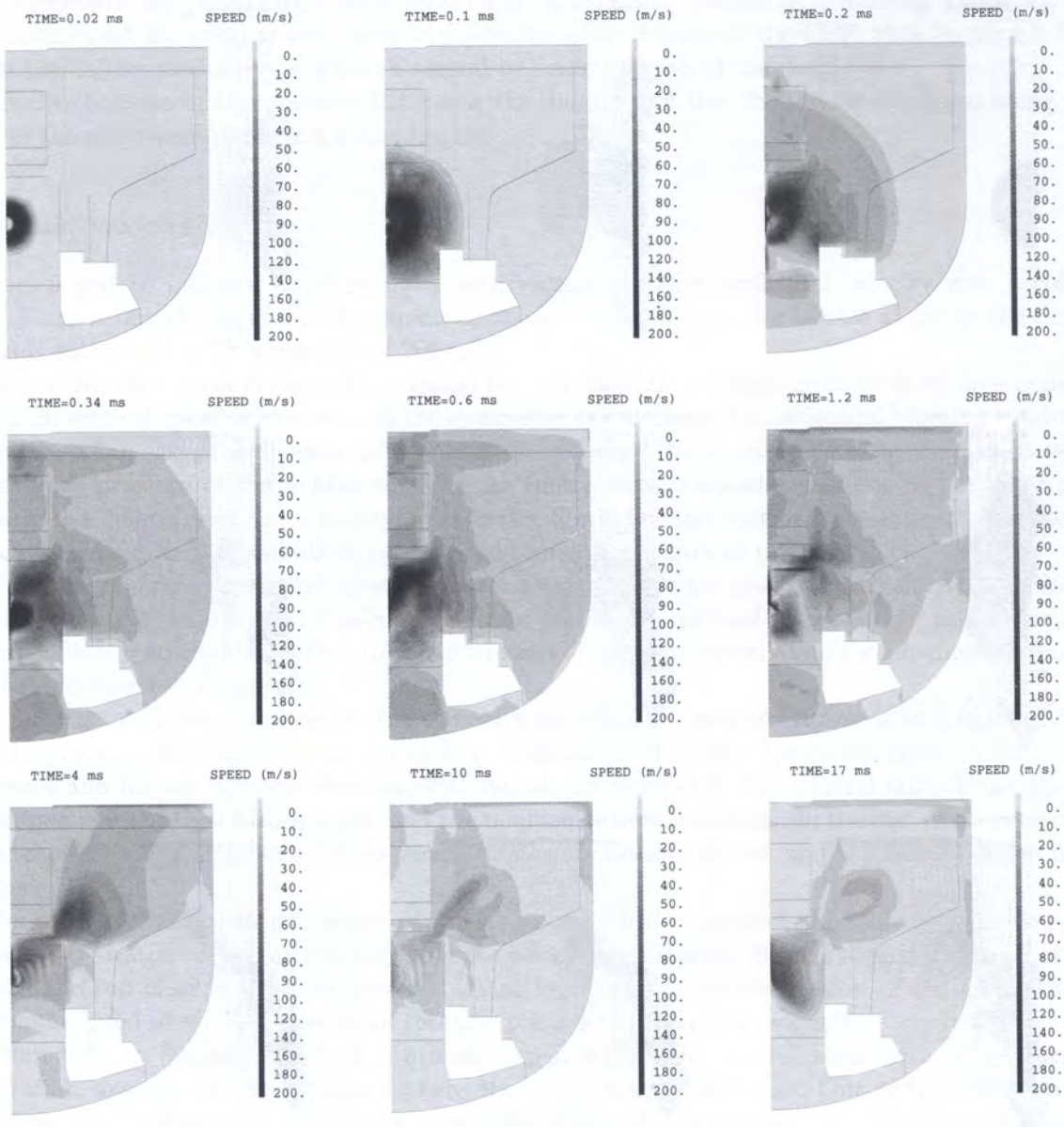

Fig. 10. Fluid speed

From 6 to 8 ms, a jet of bubble gas is violently expelled from the central area at 90 m/s and extends above the baffle. The jet sucks up the water between the neutron shielding and the internal vessel, and pushes inwards the water along the CCP external cylinder. In the CCP, water continues to be hurled upwards with slower velocities and slightly towards the symmetry axis.

In the lower part of the mock-up, water rebounds on the main vessel and flows back towards the diagrid and the internal vessel. A layer of water slides upwards along the main vessel towards the channel between both vessels. As water enters in the aforesaid channel by the bottom and argon coming from the corner by the top, the contact of both flows causes a violent splashing that succeeds in deforming the main vessel.

From 9 to 13 ms, a large whirlpool forms above the baffle. The bubble is ejected diagonally through the free channel, then it turns down at about mid-radius of the mock-up because the bubble progression is stopped by the limited capacity of water to compress. The whirlpool attracts water from the whole upper part of the mock-up and from the spaces between the neutron shielding

and the internal vessel. The highest speeds are still noted for the bubble jet but they remain limited to 40 m/s.

Simultaneously, a second smaller whirlpool appears in the central zone: part of the bubble gas flowing towards the free channel is deviated inwards along the in-pile shell; arrived near the symmetry axis, the gas flows downwards and then the cycle starts again. In the channel limited by both vessels, the direction of the fluid flows is imposed by the fluid coming from the roof. Therefore water changes direction and flows down in the channel and along the main vessel. Elsewhere, the water flows become very slowed down.

Below the roof, two contradictory fluid flows occur: argon moves outwards next to the roof whereas, a bit lower, argon and water are pulled inwards by the large whirlpool. In the CCP, the upwards water flow stops and turns back: water and argon are then propelled downwards.

Between 14 and 17 ms, the main whirlpool turns away independently from the rest of the fluid. Not only it prevents the going out of more gas from the central area but also it pushes down fluid inside the confined area. The bubble gas in the central area remains confined in that area; fluid mainly flows downwards and splashes against the diagrid. This impact on the diagrid accelerates the water below the diagrid downwards. As the fluid entering in the central area exerts an upward thrust on the CCP, the water inside the CCP changes direction and flows up once again. At the CCP top, water escapes out of the CCP whereas argon concentrates near the symmetry axis.

The main whirlpool pulls water and argon from the top closure, the internal vessel and the external cylinder surrounding the CCP. At the bottom, it pushes water inside the spaces between the neutron shielding and the internal vessel base. At the top of the channel limited by the two vessels, part of the argon flows back inwards over the top of the internal vessel and the rest expands down along the main vessel.

4.4. Deformed shape and displacements

The deformed shape of the mesh and structures are displayed versus time in Figs. 11 and 12. Figures 13 and 14 show the radial and vertical displacements of structures.

The first structures to deform at 0.2 ms are the closest ones to the explosive charge, namely the lower part of the neutron shielding and the baffle, the diagrid and the in-pile plate of the Core Cover Plug. The neutron shielding and the baffle move away while the in-pile shell is pushed up and the diagrid moves downwards. The base of the neutron shielding suffers a small downward displacement caused by the radial opening of the structure.

At 0.4 ms, the deformations of the previous quoted structures become more pronounced. The base of the main vessel starts moving down just under the diagrid, and the lower part of the internal vessel moves away. A lot of small deformations are observed in the CCP:

- All the CCP horizontal plates move up.
- The edge of the in-pile shell deforms much because of the violent thrust of the fluid trying to escape by the free channel between the in-pile shell and the neutron shielding.
- The lower part of the external cylinder and the two vertical cylinders representing the pipes buckle slightly.
- The spacer plates are lifted by their connection with the vertical cylinders: as the in-pile shell is connected to the rest of the CCP by the internal and intermediate vertical cylinders, the upward thrust exerted by the shock wave is transmitted locally by the cylinders.

Between 0.6 and 0.8 ms, owing to the water horizontal thrust, the entire neutron shielding, a large portion of the baffle and the bottom of the internal vessel move away, with a maximum radial

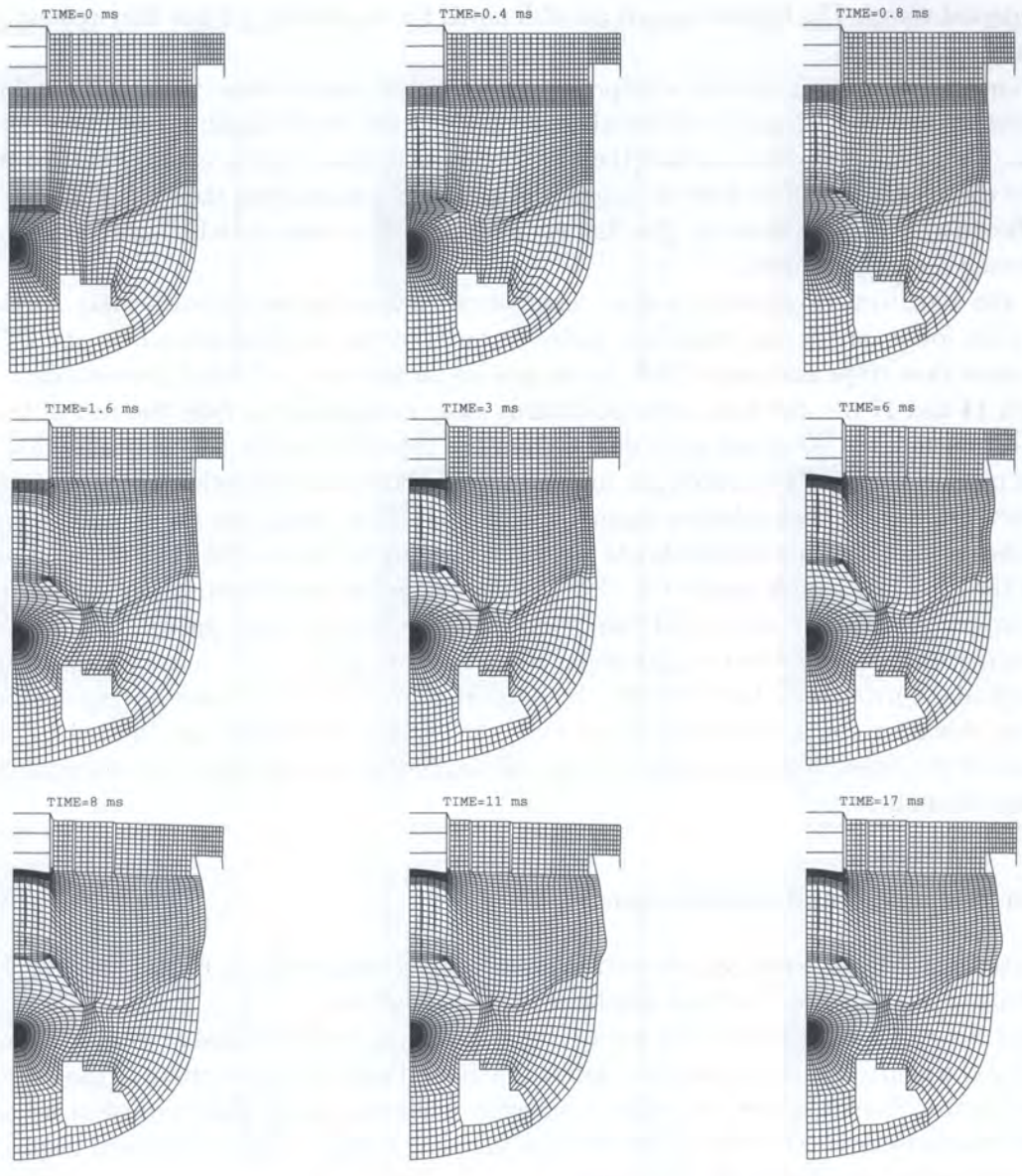

Fig. 11. Deformed shape of the mesh

displacement at charge height. This radial opening causes a slight lowering of these structures. A slight outward displacement is noted in the upper part of the internal vessel and in the main vessel a little above mid-height because of the water impact perpendicularly to both structures.

The diagrid and the vessel bottom go on lowering under the effect of the massive flows of water hurled downwards by the explosion. Almost all the rest of the main vessel starts lowering because the entire vessel is pulled down by the high thrust on its base. As the top of the vessel is vertically blocked by the embedment of the handling device, the downward deformation is proportional to the distance from the top.

The top of the main vessel moves slightly inwards near the fixing with the roof because the top closure starts going up and rotating under the impact of the upward directed water. As the massive roof slab is much more rigid than the vessel shell, the roof pulls the vessel in its rotation what explains this inward motion.

In the Core Cover Plug, the in-pile shell being pushed up, it drags in its upward motion the internal and intermediate cylinders simulating the pipes and the portion of the spacer plates between

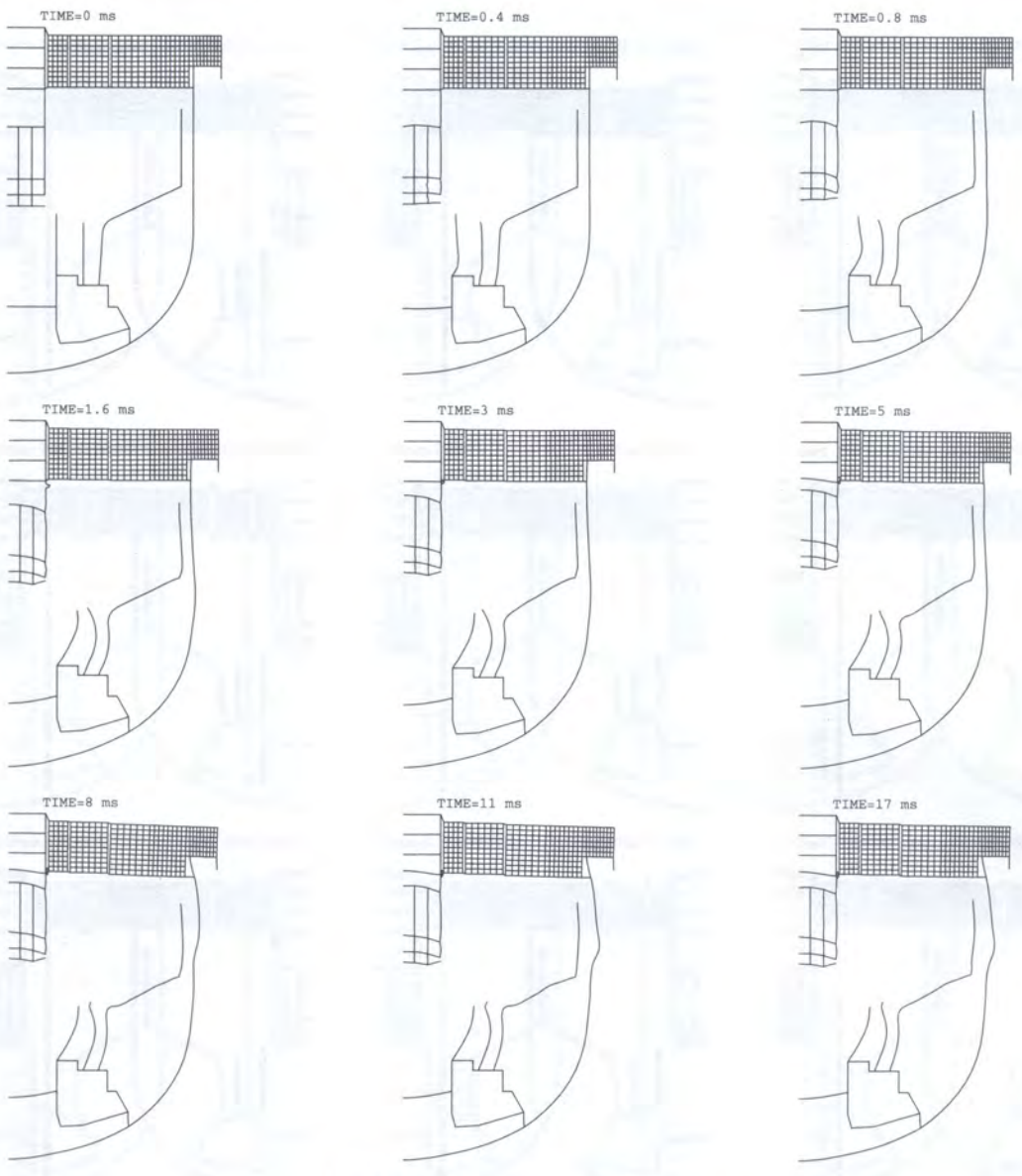

Fig. 12. Deformed shape of structures

the symmetry axis and the intermediate plate. The bending of the spacer plates pulls inwards the edges of the plates, linked to the external cylinder which does not move as it is not directly linked to the in-pile shell.

Between 1 and 1.8 ms, the neutron shielding and the baffle greatly deform because of the large bubble flows out of the central zone. The top of the neutron shielding opens completely as a flower while the baffle and the lower part of the internal vessel deform at mid-height, taking a moon shape.

The upper part of the internal vessel bends near the junction with the intermediate part owing to the massive flows of water propelled by the going out of the bubble. A lower bulge forms at the junction of the torospherical and cylindrical parts of the main vessel, due to the water flows along the main vessel and between both vessels.

The diagrid and the main vessel continue lowering. As the downward water flows hit the main vessel principally under the diagrid, the lowering of the vessel is concentrated under the diagrid, but the lowering also induces at 1 ms an extension of the vessel which pulls down and slightly inwards the part of the vessel located under the Core Support Structure. But at 1.5 ms, the inward displacement has almost desappeared because water is flowing along the vessel towards the collar;

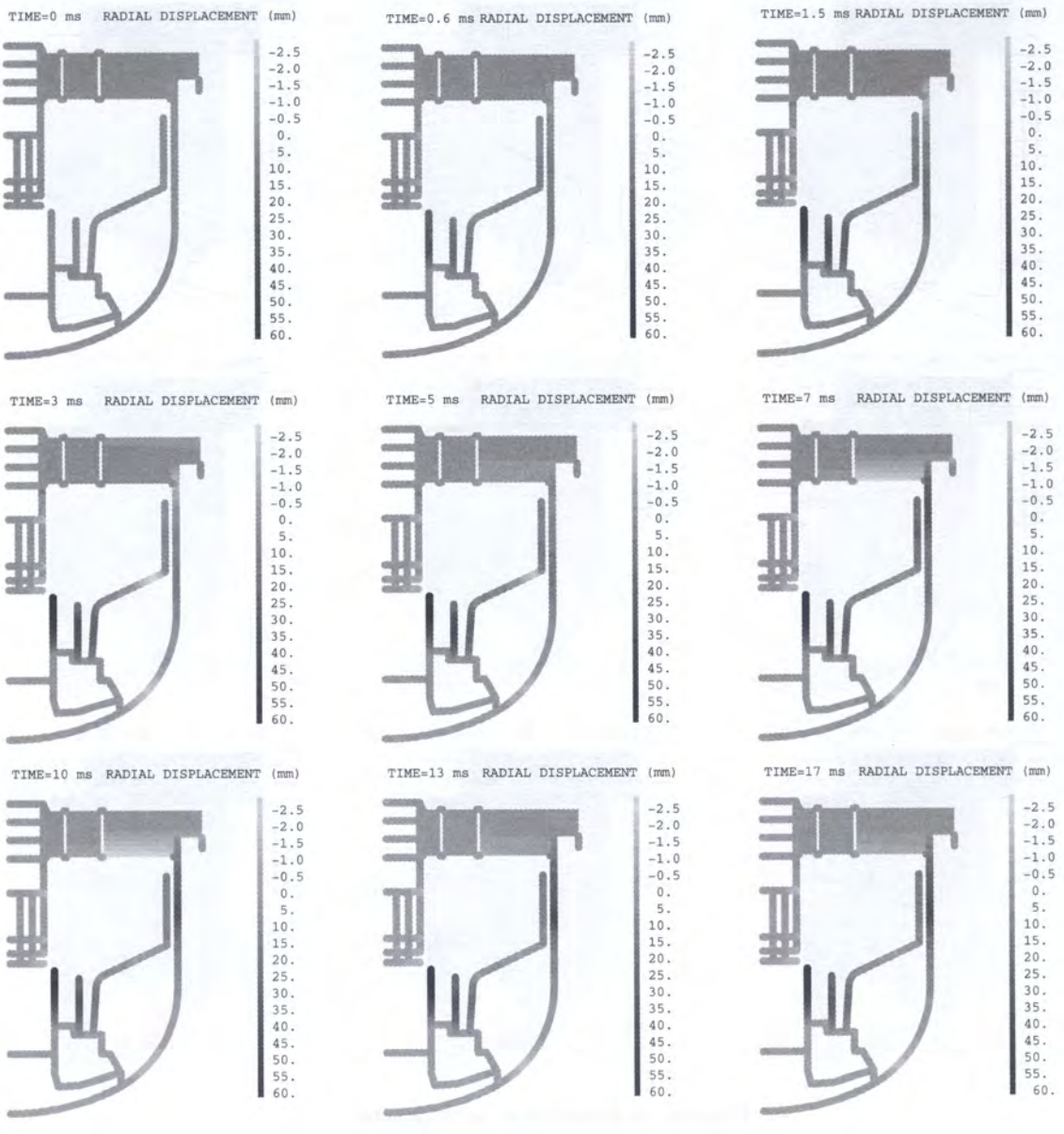

Fig. 13. Radial displacements (mm)

thus the deformation of the vessel bottom becomes more regular and the vessel bending is only vertical. Meanwhile, the CSS does not move laterally because it is supposed rigid.

In the Core Cover Plug, the in-pile shell bends both at the edge owing to the fluid escaping by the free channel and at the centre because of the vertical fluid thrust. The upward thrust of water inside the CCP stretches the internal and intermediate cylinders, so that the deformation of the spacer plates becomes more regular: the highest displacement is located at the centre and the lowest one near the external vessel. The embedment of the plates with the external cylinder induces an extra-rigidity that limits the vertical motion of the plates.

The bending of the spacer plates shifts slightly inwards the cylinders, therefore the shape of the external cylinder becomes wavy. The combination of the pulling up of the spacer plates and the splashing and rebound of water propelled against the heat-insulation causes a buckling of the external cylinder just below the top closure. The heat-insulation lower plate does not

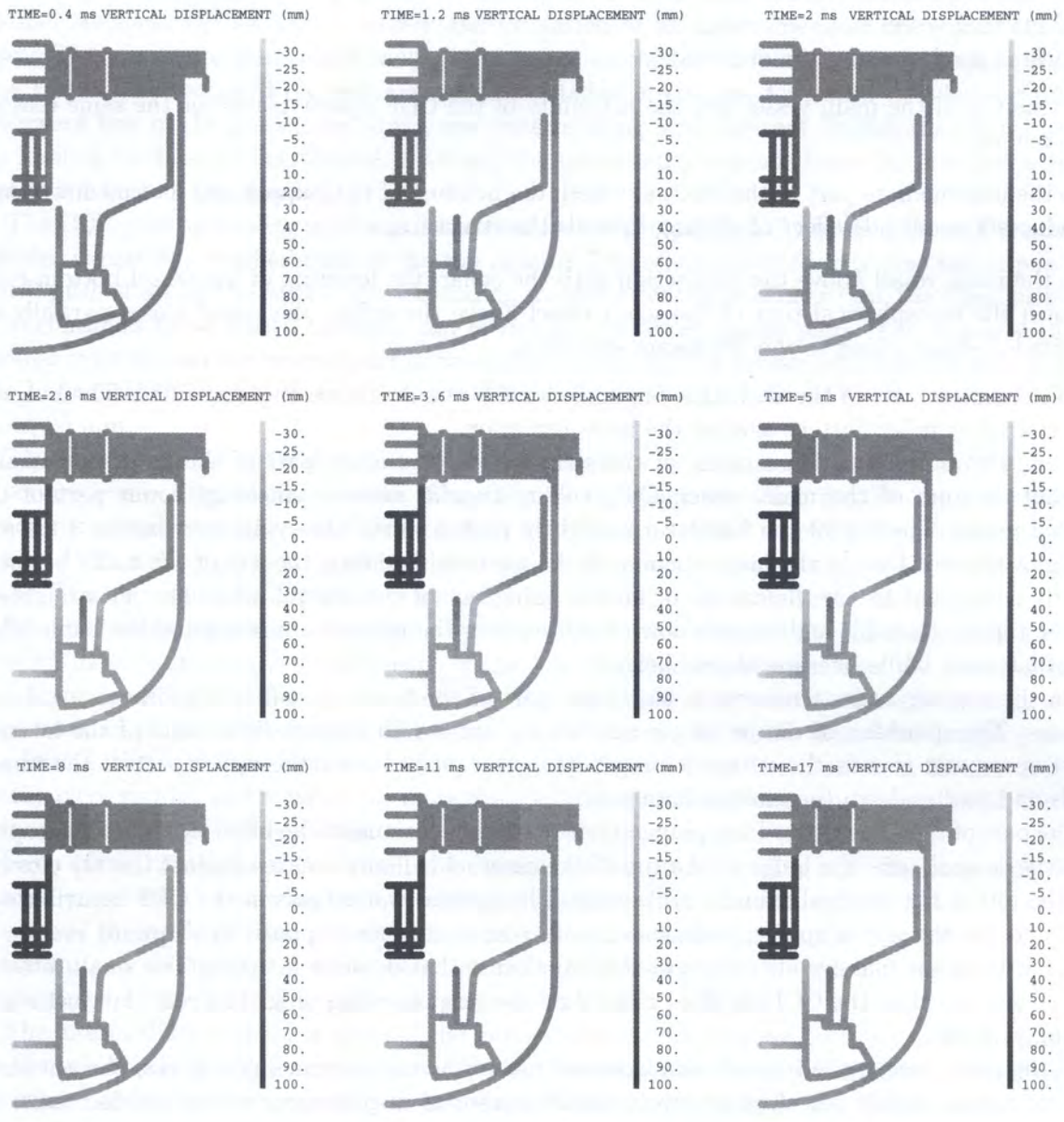

Fig. 14. Vertical displacements (mm)

bend because it is more rigid than the external cylinder. The buckling of the external cylinder brings about a shortening of the cylinder and thus a general upward displacement of the CCP.

At 2 ms, the neutron shielding, the baffle and the lower part of the internal vessel reach respectively a maximum radial displacement of 60 mm at the top, 45 mm and 25 mm half-way up. The lowering of the main vessel becomes more pronounced; in turn, the vessel pulls down the collar, the Core Support Structure, and the structures attached to the CSS: diagrid, neutron shielding, and lower part of the internal vessel. The only exception concerns the baffle: the water motions in that area involve a rounded deformation and a streching of the shell.

At 2.8 ms, maximum lowerings are observed in the centre of the diagrid (– 30 mm), at the top of the neutron shielding (– 30 mm), for the entire CSS (– 10 mm), and in the internal vessel at the junction of the lower and intermediate parts (– 20 mm). The lower bulge of the main vessel extends and reaches a maximum radial displacement of 15 mm just below the channel between both

vessels. Because of the upward water flows below the intermediate part of internal vessel, this part of the internal vessel stops lowering.

Inwards displacements are observed:

- at the top of the main vessel and the extremity of the CCP spacer plates for the same reasons as before,
- in the intermediate part of the internal vessel: the bending of both upper and intermediate parts induces a small side effect of shifting inwards the structure,
- in the main vessel above the connection with the collar: the lowering of the vessel bottom pulls down the torospherical part of the main vessel above the collar; the vessel looses partially its rounded shape owing to the downward extension.

The complete part of the CCP that is plunged inside the fluid goes on being lifted. The bulge of the external cylinder flattens against the heat-insulation.

From 3 to 5 ms, the deformation of the structures in the lower part of the mock-up remains constant: bottom of the main vessel, CSS, collar, diagrid, neutron shielding, lower part of the internal vessel. The top of the baffle turns slightly back towards the symmetry axis at 3 ms and then moves away. Due to the large opening of the neutron shielding, the top of the baffle becomes directly submitted to the violent jet of bubble going out of the central area. The jet straightens out the top of the baffle and propels down fluid between the neutron shielding and the baffle what accentuates the baffle bending at mid-height.

On the contrary, the structures in the upper part of the mock-up suffer large increasing deformations. The splashing of the jet of gas against the upper and intermediate parts of the internal vessel opens and rounds the corner joining both parts, pushes away the upper part of the vessel, bends and pushes down the intermediate part.

The part of the Core Cover Plug plunged into the fluid continues to be lifted by the fluid escaping from the central area: the bulge at the top of the external cylinder crashes against the top closure, and the top of the external cylinder still bends. The upward water flows in the CCP contribute to bend and lift the upper spacer plate and the heat-insulation lower plate. The upward motion of the CCP pulls the massive structures of the top closure that deforms in stairs. The small rotating plug, located next to the CCP, is lifted more than the large rotating plug. The roof slab just starts moving at 5 ms.

In the main vessel, the inwards displacement above the collar connection grows, the outwards displacement at mid-height does not evolve and the inwards displacement at the top decreases.

From 6 to 9 ms, the bottom of the main vessel and the diagrid stop lowering and move back upwards due to the rebound of water against the vessel bottom and the reversal of the water flow under the diagrid. In its upward motion, the vessel bottom pulls up the rest of the main vessel, the collar and the CSS, as well as the neutron shielding, the baffle and the internal vessel lower part.

The radial displacement of the neutron shielding remains constant. The top of the baffle opens and tilts outwards for two reasons. Firstly, the bubble jet impacts directly the top of the baffle. Secondly, the fluid previously pushed down between the baffle and the shielding rebounds against the CSS, flows back up, and forces the baffle top to move away when going out of the space between both shells.

The radial displacements decrease in the lower and intermediate parts of the internal vessel because the fluid flows below the internal vessel change direction. The internal vessel is impacted from below by water that has rebounded against the main vessel. However, the upper part of the internal vessel moves a bit more away, since fluid is propelled almost horizontally against the internal vessel upper part. The radial displacement reaches a maximum of about 15 mm at 7 ms. In addition, the fluid flows passing over the internal vessel to go inside the channel between the two vessels push the top of the internal vessel that bends inwards and moves down.

The compression of the argon bag in the top right-hand corner and its flowing down in the channel between the two vessels causes the formation of an upper bulge at the top of the main vessel. The top of the main vessel moves away, what extends the rubber-ring band joining the roof base to the main vessel. Progressively, the upper bulge progresses downward in relation with the downward flow of the pressurised argon and water coming from the roof, to join the lower bulge at the level of the base of the channel. At 9 ms, the upper bulge extends from the junction with the roof to the base of the channel.

The CCP goes on moving up towards the heat-insulation, particularly in the centre. The external cylinder is partially crashed against the top closure. The reason of this lift is that the in-pile shell is still pushed up by the bubble gas expanding from the central zone and that the fluid inside the CCP continues to be hurled upwards and to impact the upper spacer plate. The in-pile shell, the internal cylinder and the central part of the spacer plates reach a maximum lift of 100 mm at 9 ms. The lower heat-insulation plate is lifted of 30 mm, and the other plates of the heat-insulation of about 20 mm.

The upward thrust of fluid on the top closure leads to an important deformation of the set of structures composing the top closure. Since the joining rings are much flexible than the massive structures, the pieces of the roof shift up mainly at the ring level, and a deformation in stairs appears clearly. The rotating plugs keep their original shape whereas the joining rings are completely out of shape. The maximum displacement reaches 20 mm at 9 ms in the small rotating plug.

The roof slab rotates around the locked point at the bottom extremity of the hanging device. The rotation induces an inward displacement of the top closure, more marked near the external radius than in the centre. That rotation explains the inward displacement recorded at the bottom of the large rotating plug, on the lower half-height of the roof slab and at the top of the hanging device. In addition, the roof slab deforms slightly at the level of the two pieces of different thicknesses. The thicker piece rotates and moves a bit more than the thinner: this phenomenon is visible at the base of the vertical line of elements that is stretched between 5 and 9 ms.

From 10 to 12 ms, the main vessel, the diagrid, the neutron shielding and the lower part of the internal vessel keep on moving back upwards because the water flows slow down below the diagrid. The top of the baffle is lifted and deforms more or less like rubber under the effect of the whirlpool formation and the upward flow between the neutron shielding and the internal vessel. The radial displacement of the top of the baffle increases up to 25 mm at 12 ms.

The intermediate and upper parts of the internal vessel slightly move both upwards and inwards. On the one hand, the fluid flowing down in the channel pushes back the upper part inwards. On the other hand, the intermediate part bends up at mid-length because the fluid coming from the channel and flowing below the plate lifts the plate.

The upper bulge in the main vessel takes a pointed shape just above the level of the channel between both vessels. The bulge reaches a maximum extent of 35 mm at 12 ms. The formation of this bulge contributes to pull up the portion of the vessel located between the collar and the bottom of the channel.

In the core cover plug, as the fluid flows reverse and orient downwards, the spacer plates are pushed down. Therefore the entire CCP moves back down, and the lower spacer plate and the in-pile shell come closer at the centre and at the edge. The internal and intermediate cylinders succeed nevertheless in maintaining a certain distance between both plates at mid-radius of the CCP.

The fluid being attracted from below the top closure by the whirlpool, the compression of the top closure stops and the structures move back. The inward displacements decrease in the top closure as the closure rotates back.

From 13 to 16 ms, the whirlpool pushes violently fluid inside the central area. The fluid impacts the diagrid which lowers again. In turn, the water below the diagrid is accelerated downwards. When it impacts the vessel bottom, the vessel lowers again, what pulls down the rest of the main vessel and the structure set attached to it.

Since the top closure moves slightly back downwards, the hanging device stops rotating and turns back. The inward radial displacement of the top closure decreases in the roof slab, and completely desappears in the large rotating plug and the hanging device.

The downward water flows in the CCP slightly lower the entire CCP, and especially the upper spacer plate that moves away from the heat-insulation.

From 16 ms, the fluid inside the CCP rebounds against the spacer plates and flows up a second time. In parallel, the fluid propelled inside the central area pushes upwards the CCP base. Consequently the entire CCP (spacer plates, cylinders and heat-insulation) moves up another time. The pressurised fluid escapes by the perforated part of the external cylinder below the top closure and spreads under the top closure which moves up again.

4.5. Von Mises stresses in the structures

Figure 15 shows the stresses in the external and internal structures. The first stresses appear in the neutron shielding, the in-pile shell and the bottom of the internal and intermediate cylinders of the CCP. They correspond to the impact of the pressure wave on the structures limiting the central area.

At 0.2 ms, the baffle, the lower part of the internal vessel, and the complete part of the CCP plunging into the fluid undergo stresses. The diagrid is spared because it is connected to the CSS by a swivel contact, it can rotate and bend freely. Local higher values are recorded at the junctions between the plates and cylinders of the CCP since the load exerted in the central zone is transmitted to the spacer plates via the cylinders.

At 0.3 ms, new zones undergo stresses: the bottom of the main vessel, the intermediate part of the internal vessel, and the ring joining the upper heat-insulation plate to the top of the small rotating plug due to the upwards lift of the CCP. Simultaneously, stresses decrease in the CCP internal cylinder and in the centre of the spacer plates, thus following the pressure decrease in that area.

From 0.4 to 0.5 ms, as water is hurled violently against structures with speeds of about 20 m/s, stresses increase in the already quoted structures, and appear in the upper part of the internal vessel, the collar and the main vessel up to the roof. Stresses reach a maximum of 600 MPa at the bottom of the main vessel.

High-stress spots appear:

- in the main vessel at the collar attachment,
- at the junction between the torospherical and the cylindrical pieces of the main vessel due to the different thicknesses of the vessel in both parts,
- at the connections between the plates and cylinders of the CCP, owing to the upward thrust of fluid in the central area.

The ring joining both rotating plugs of the top closure become submitted to stresses: the water impacting the top closure deforms the rings rather than the massive structures as the massive pieces are very strong and rigid. No stresses are observed in the Core Support Structure as it is very thick. Stresses remain limited in the diagrid support because the constitutive law of this structure presents a very low plastic threshold. They decrease in the intermediate cylinder of the CCP as it is not coupled to fluid.

From 0.6 to 1.2 ms, stresses increase:

- in the neutron shielding and the baffle because the bubble starts escaping out of the central zone,

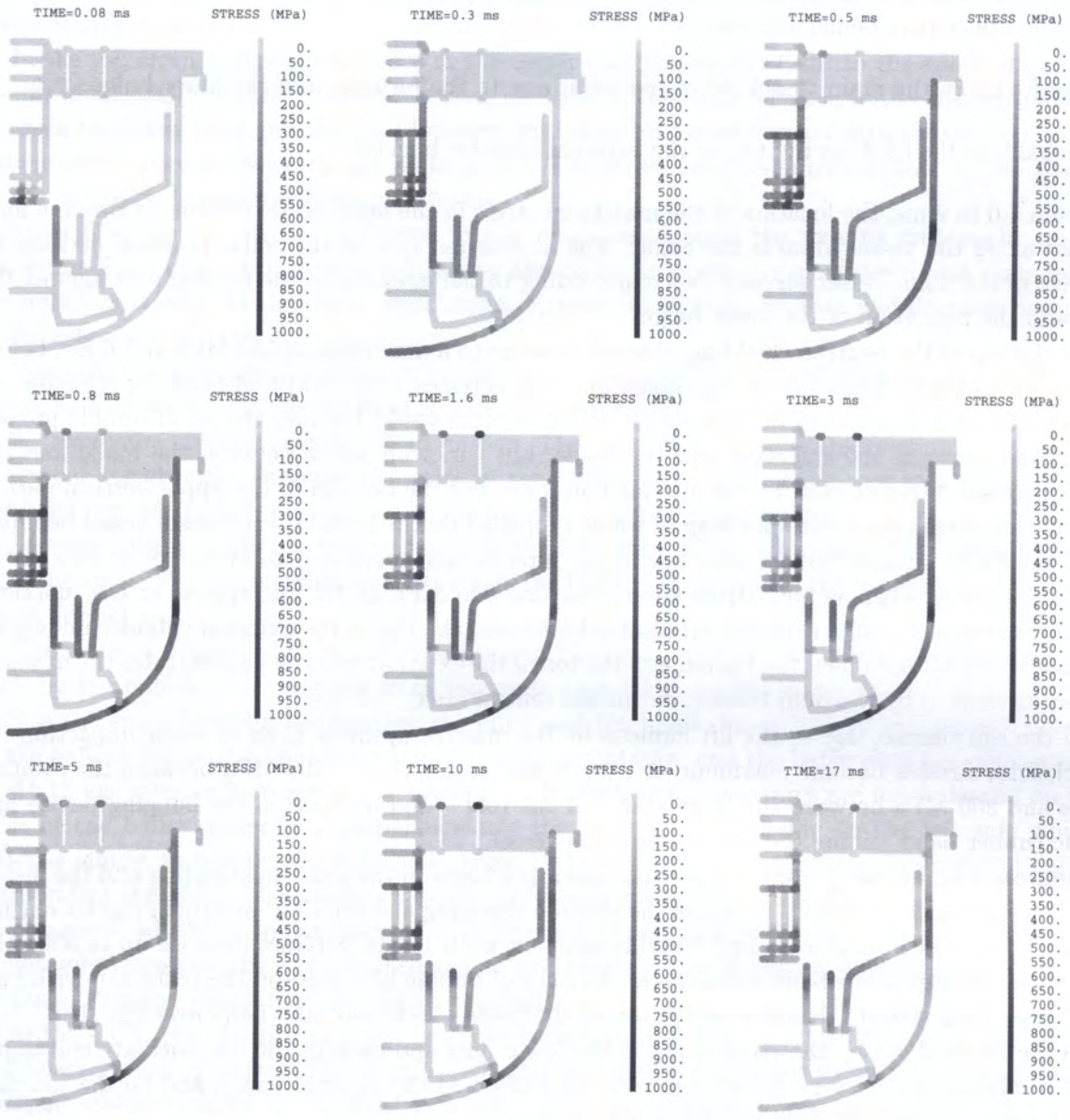

Fig. 15. Stress (MPa)

- at the bottom of the main vessel, up to 600 MPa at 0.8 ms, because water is continuously hurled against the vessel bottom from 0.3 ms,
- in the collar where a high-stress spot appears because the connection of the main vessel with the rigid CSS prevents a free deformation of the vessel under the water thrust,
- at 0.8 ms, in the main vessel above the collar, because of the splashing of water against the vessel,
- in the joining rings, owing to the high thrust of the fluid hurled against the top closure,
- in the hanging device because the upwards flows make rotate the top closure around the fixed extremity of the hanging device.

Stresses remain unchanged in the lower part of the internal vessel. They decrease:

- in the intermediate part and at the top of the upper part of the internal vessel because the base of the upper part bends and recoils,
- from 1 ms in the main vessel above the collar due to the formation of the lower bulge,
- globally in the CCP as the top of the external cylinder buckles.

From 1.6 to 2 ms, the location of the maximum stress in the main vessel bottom follows the fluid impact along the vessel towards the collar. The high-stress spot at the collar junction persists. In the rest of the main vessel, stresses evolve according to the intensity of the fluid impact against the wall and the formation of the lower bulge.

At the top of the neutron shielding, stresses raise up to a maximum of 650 MPa at 1.6 ms, before decreasing as the shell reached its maximum opening. Stresses increase at mid-height of the baffle up to 550 MPa and decrease in the lower part of the internal vessel because the jet of bubble propels down fluid between the shielding and the baffle, but sucks up water between the baffle and the internal vessel. Stresses raise in the intermediate part and the bottom of the upper vertical part of the internal vessel, since the splashing of water propelled by the bubble jet causes a vessel bending.

In the CCP, stresses remain very low in the internal and intermediate cylinders, reduce in the horizontal plates whereas high-stress spots, reaching 750 MPa at 1.6 ms, appear at the junctions of the three spacer plates with the external cylinder and the top of the external cylinder undergoes stresses of 500 MPa. In fact, the buckling of the top of the external cylinder concentrates the upwards strengths exerted by the fluid flowing out of the central area.

In the top closure, due to the lift induced by the massive upwards flows of water impacting the top closure, stresses become maximum at 2 ms in the joining rings – 500 MPa between the rotating plugs and 800 MPa between the large plug and the roof – and increase in the hanging device and in the rubber band joining the roof to the main vessel.

Between 3 and 5 ms, the stress level becomes much lower in the neutron shielding and the in-pile shell since the space between the top of the neutron shielding and the CCP external cylinder reaches its maximum width from 3 ms and remains constant until 10 ms. Stresses increase up to 550 MPa at 3 ms at the top of the baffle because the panache of bubble hits head-on the baffle top with high velocities. Then stresses decrease as the top of the baffle bends and fluid flows over the shell.

In the internal vessel, the stresses fall in the lower part and raise in the intermediate and upper parts because flows are very limited between the baffle and the internal vessel, and on the contrary massive and violent in the upper part of the mock-up.

Below the diagrid, water rebounds against the main vessel bottom and the collar at 3 ms and then flows back sideways and upwards. Consequently, a maximum stress of 600 MPa is observed in the collar vicinity at 3 ms, then the local maximum stress in the vessel moves back towards the axis, and finally stresses reduce in the vessel. The deformation of the collar absorbs partially the water impact, so that the reflected wave is lower than the incident one, and the stress level is lower in the main vessel at 4 ms than at 3 ms.

Above the collar, stresses increase until 3 ms, time when water bounces back against the vessel. Then they decrease regularly as water flows away from the vessel. Above mid-height, water forces the base of the channel between both vessels to flow up, so that stresses concentrate below the channel at 3 ms and then increase in the upper part of the main vessel.

In the CCP, the stress level is rather low, except at the connections of the horizontal plates with the external cylinder. The lift of the spacer plates being limited by their attachment with the external cylinder, stresses concentrate at the connections between the plates and the cylinder. As the top of the external cylinder ends crashing against the top closure at 3 ms, a high-stress spot appears at 4 ms at the junction with the heat-insulation. Afterwards, as fluid escapes laterally by

the upper part of the CCP, stresses decrease both in the heat-insulation and at the top of the external cylinder.

In the top closure, stresses increase in the upper ring joining the CCP to the small plug due to the lift of the CCP. On the contrary, stresses decrease in the rings between both rotating plugs and between the large plug and the roof because fluid does no longer impact directly the top closure, but deviates sideways towards the main vessel. The stress level remains constant in the hanging device as the roof temporarily stops rotating.

From 6 to 17 ms, stresses decrease in the main vessel from the axis to mid-height because the water flows below the diagrid and above the collar progressively slow down and their impact becomes less strong. At the collar attachment, stresses alternately increase and decrease according to the rebounds of water.

However, the cylindrical upper part of the main vessel continues to suffer stresses up to 600 MPa at the level of the channel; as the fluid coming from the roof moves down in the channel, the location of the maximum stress follows the fluid motion. The maximum stress is observed at the location of the upper vessel bulge. Stresses also raise in the rubber band joining the roof to the main vessel: the band extends from 6 ms because of the formation of the upper bulge.

Stresses reduce in the internal vessel: with the formation of the whirlpool, the fluid is attracted from the vicinity of the internal vessel towards the baffle. Consequently the pressure exerted on the vessel decreases.

The baffle is submitted to high stresses (up to 600 MPa) at 6 ms. At that time, the baffle is hit both by the bubble gas going out from the central zone and by the water that rebounded on the CSS in the space between the neutron shielding and the baffle. From 7 to 10 ms, stresses decrease in the baffle because the fluid flows keep the same orientation and the baffle does not deform more.

At 12 ms, stresses increase at the base of the baffle because pressures are not balanced on both sides of the baffle: water hits perpendicularly the bottom of the baffle on the left side whereas water is almost at rest on the right side. From 14 to 17 ms, fluid flows down again in both spaces surrounding the baffle, what causes a stress increase in the rest of the baffle.

The small whirlpool in the internal zone exerts a thrust against the neutron shielding at mid-height, what explains the stresses observed at mid-height of the shielding. The stress level depends on the orientation of the fluid impacting the shell.

In the CCP, the absence of fluid-structure coupling generates very low stresses in the internal and intermediate cylinders. The in-pile shell and the spacer plates are submitted to more or less constant stresses caused by the fluid twirling in the central zone. The stress concentration at the right extremities of the spacer plates is linked to the large whirlpool.

In parallel with the vertical lift in stairs of the top closure, stresses increase in the joining rings and the hanging device between 6 and 10 ms. They decrease from 12 ms as the fluid flows back downwards and the top closure moves back down. The highest stresses (900 MPa) are observed in the ring between the roof and the large rotating plug: as the roof slab is larger than the three plugs, its deformation is more limited than the one of the plugs and thus the strain of the nearest ring is higher.

The stress level remains very low in the rigid structures (massive structures of the top closure, thick shell such as the CSS). In the diagrid support, the stresses remain limited because the structure becomes almost immediately plastic and suffers large deformations compared to the stress level.

4.6. Plastic strains in the structures

Figure 16 shows the plastic strains in the structures versus time. At 0.2 ms, the entire neutron shielding undergoes plastic strains and the baffle starts becoming plastic. Strains are due to the impact of the shock wave on these structures from respectively 0.06 and 0.1 ms.

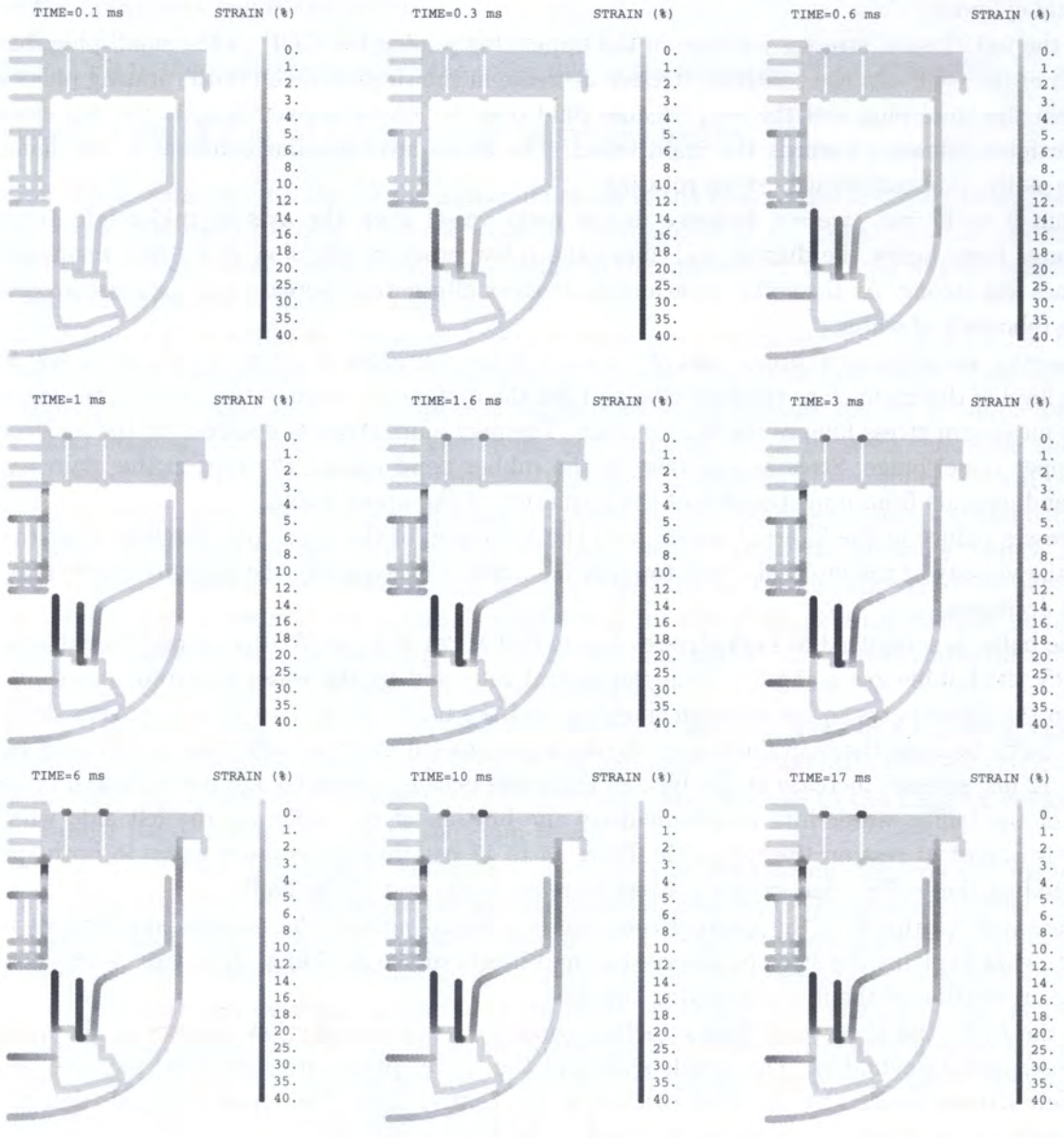

Fig. 16. Strain (%)

At 0.3 ms, the plastic strains increase in both structures and appear at the edge of the diagrid, on the CSS side. As the diagrid is relatively thick, its deformation is much lower than that of the neutron shielding. The in-pile shell, the lower and upper spacer plates, as well as the lower part of the external cylinder present low plastic strains, due to upward rising of the CCP pushed up by the shock wave.

From 0.4 to 0.8 ms, the strain level raises in the previous structures because they are included in the pressurised area. In addition, the part of the main vessel under the diagrid becomes plastic because the shock wave hits it at 0.26 ms and, from this instant the water under the diagrid is propelled towards the vessel.

The lower part of the internal vessel and the upper part of the main vessel undergo plastic strains from 0.4 ms and 0.6 ms: they are impacted by the shock wave from 0.14 ms and 0.34 ms, respectively. In the CCP, the junction of the spacer plates with the external cylinder become plastic

respectively. In the CCP, the junction of the spacer plates with the external cylinder become plastic at 0.6 ms; the plates present a high bending from 0.8 ms because of the violent thrust of the fluid below the CCP.

Between 1 and 1.2 ms, the plastic level increases strongly in the neutron shielding, the baffle and the diagrid support, and more moderately in the lower part of the internal vessel, the CCP, the bottom and the cylindrical part of the main vessel. Plastic strains appear in the external cylinder of the CCP below the heat-insulation, when the shell buckles. The ring joining the two rotating plugs becomes plastic due to the high fluid thrust under the top closure.

Between 1.6 and 5 ms, the strain level raises mainly in the neutron shielding, the baffle, the ring between both rotating plugs and the junction of the CCP external cylinder with the heat-insulation plate. The strain level reaches a maximum of 40% at 1.6 ms at the top of the neutron shielding, 30% at 2.2 ms at mid-height of the baffle, 8% in the centre of the diagrid support and in the lower part of the internal vessel at 1.6 ms and 4 ms, respectively.

Plastic strains appear:

- from 1.6 ms in the ring joining the large plug to the roof due to the sideways flow of water and argon from the CCP towards the main vessel,
- from 3 ms in the heat-insulation plate at the junction with the cylinder, with a maximum strain level of 5% reached at 5 ms,
- at 4 ms in the centre of the heat-insulation plate.

From 6 to 17 ms, the plastic strains remain constant in the shielding, the baffle, the diagrid, the main vessel bottom and the majority of the CCP. On the contrary, they increase:

- in the internal vessel at the junction between the lower and intermediate parts because the whirlpool causes a bending of the intermediate part,
- in the cylindrical part of the main vessel because of the formation of the upper bulge: they extend from the top to the bottom of the cylindrical part of the main vessel due to the fluid flowing from the roof to the base of the channel, and a uniform plastic strain of about 8% is reached in the main vessel at the height of the channel,
- in the two rings joining the rotating plugs and the roof slab, because of the fluid flows below the top closure generated by the whirlpool; maximum plastic strains of 14% and 20% are observed at 14 ms, respectively in the ring between the small and large rotating plugs and between the large plug and the roof slab.

5. Conclusion

This paper presents a computation of a Hypothetical Core Disruptive Accident in the MARS mock-up. This mock-up is a small-scale replica of a Fast Breeder Reactor, and contains all the internal structures of the reactor block. The fluids intervening in the real accident were replaced by water, argon and an explosive charge in the experiment.

In the numerical model, the majority of the structures are represented by shells or massive structures. However, the internal structures of complex geometry in the area of the internal vessels are simply taken into account by a pressure loss. The internal fluids are described by the specific CDA constitutive law implemented on purpose in the EUROPLEXUS code to be able to simulate this kind of explosion.

The explosive wave propagates from the centre of the mock-up towards the main vessel and the top closure. The passing of the pressure wave loads and deforms the internal structures and then the external ones. The structures most in demand are the neutron shielding and the core cover plug because of their proximity with the pressurised area.

The high-pressure gas bubble expands from the central part of the mock-up to the rest of the mock-up, thus pushing away the top of the neutron shielding and the in-pile shell. The argon layer under the top closure is compressed below the roof and pushed in the channel between the internal and main vessels. A bulge forms in the upper part of the main vessel during the passing of the pressurised fluid in the channel.

During the explosion, the water contained into the mock-up is accelerated and hurled against the structures. In particular, the water impacts perpendicularly the main vessel and the top closure. The water thrust leads to a large deformation of the bottom of the main vessel. The fluid impacting the top closure causes a deformation in stairs (more important at the centre than at the edge) linked to the lower rigidity of the joining rings than that of the massive slabs (plugs and roof).

A comparison of the computed results with the experimental results, and previous results issued from the CASTEM-PLEXUS code will be presented in another paper. In addition, a new HCDA model taking into account the presence of the internal structures (without meshing them) by means of an equivalent porosity method [44] will be tested to understand the influence of the peripheral structures (pumps, heat exchangers) on the containment response.

References

[1] D. Acker, A. Benuzzi, A. Yerkess, J. Louvet. MARA 01/02 – Experimental validation of the SEURBNUK and SIRIUS containment codes. *Proc. 6th Int. Conf. on Structural Mechanics In Reactor Technology*, Paper E 3/6, Paris, France: August 1981.

[2] C. Albertini, et al. The JRC-COVA programme : Final Report. Commission of the European Communities, Report EUR 8705, 1983. *Nuclear Science and Technology*: 1–182, 1984.

[3] A. Benuzzi. Comparison of different LMFBR primary containment codes applied to a benchmark problem. *Nuclear Engineering and Design,* **100**: 239–249, 1987.

[4] Y. Blanchet, P. Obry, J. Louvet. Treatment of fluid-structure interaction with the SIRIUS computer code. *Proc. 6th Int. Conf. on Structural Mechanics In Reactor Technology*, Paper B 8/8, Paris, France: August 1981.

[5] C. Bour, M. Spérandio, J. Louvet, C. Rieg. LMFBR's core disruptive accident. Mechanical study of the reactor block. *Proc. 10th Int. Conf. on Structural Mechanics In Reactor Technology*, Anaheim, USA, Vol. E: 281–287, August 1989.

[6] H. Bung, F. Casadei, J.P. Halleux, M. Lepareux. PLEXIS-3C: A computer code for fast dynamic problems for structures and fluids. *Proc. 10th Int. Conf. on Structural Mechanics In Reactor Technology*, Vol. B: 85–90, Anaheim, USA, August 1989.

[7] I.G. Cameron, B.C. Hankin, A.G.P. Warham, A. Benuzzi, A. Yerkess. The computer code SEURBNUK-2 for fast reactor explosion containment safety studies. *Proc. 4th Int. Conf. on Structural Mechanics In Reactor Technology*, Paper B 2/1, San Francisco, USA: August 1977.

[8] Y. Cariou, M. Spérandio, M. Lepareux, K. Christodoulou. LMFBR's whole core accident. Validation of the PLEXUS code by comparison with MARA tests. *Proc. 12th Int. Conf. on Structural Mechanics In Reactor Technology*, Paper E 7/4, Stuttgart, Germany: August 1993.

[9] Y. Cariou, J.P. Pirus, C. Avallet. LMR large accident analysis method. *Proc. 14th Int. Conf. on Structural Mechanics In Reactor Technology*, Paper P 3/7, 395–402, Lyon, France: August 1997.

[10] Y. Cariou, M. Lepareux, H. Noé. LMR's whole core accident. Validation of the PLEXUS code by comparison with MARS test. *Proc. 14th Int. Conf. on Structural Mechanics In Reactor Technology*, Paper P 2/6, 339–346, Lyon, France: August 1997.

[11] F. Casadei, A. Daneri, G. Toselli. Use of PLEXUS as a LMFBR primary containment code for the CONT benchmark problem. *Proc. 10th Int. Conf. on Structural Mechanics In Reactor Technology*, Paper E 13/1, 299–304, Anaheim, USA: August 1989.

[12] Y.W. Chang, J. Gvildys, S.H. Fistedis. Analysis of the primary containment response using a hydrodynamic-elastic-plastic computer code. *Nuclear Engineering and Design,* **27**: 155–175, 1974.

[13] Y.W. Chang. Application of containment codes to LMFBRs in the United States. *Nuclear Engineering and Design,* **42**: 53–67, 1977.

[14] C. Chavant, A. Hoffmann, P. Verpeaux, J. Dubois. Plexus: A general computer code for explicit Lagrangian computation. *Proc. 5th Int. Conf. on Structural Integrity In Reactor Technology*, Paper B 2/8, Berlin, Germany, 1979.

[15] M. Cigarini, A. Daneri, G. Toselli. Applications of ASTARTE-4 code to explosive models with complex internal structure using the rezoning facility. *Proc. 7th Int. Conf. on Structural Mechanics In Reactor Technology*, Paper B 9/3, Chicago, USA, August 1983.

[16] M.S. Cowler, S.L. Hancock. Dynamic fluid-structure analysis of shells using the PISCES 2 DELK computer code. *Proc. 5th Int. Conf. on Structural Mechanics In Reactor Technology*, Paper B 1/6, Berlin, Germany, 1979.

[17] A. Daneri, G. Toselli, T. Trombetti, Y. Blanchet, J. Louvet, P. Obry. Influence of the representation models of the stress-strain law on the LMFBR structures in an HCDA. *Proc. 6th Int. Conf. on Structural Mechanics In Reactor Technology*, Paper E 4/4, Paris, France, August 1981.

[18] F. David. Etude d'une composition explosive flegmatisée. Applications à la deformation d'une cuve. *Proc. Symposium sur les hautes pressions dynamiques*, Paris, France, 1978.

[19] M. Falgayrettes, C. Fiche, P. Granet, P. Hamon, P. Barrau, B. Magnon, J. Jalouneix, M. Nédélec. Response of a 1/20 scale mock-up of the Superphenix breeder reactor to an HCDA loading simulation. *Proc. 7th Int. Conf. on Structural Mechanics In Reactor Technology*, Paper E 4/1, 157–166, Chicago, USA, 1983.

[20] C. Fiche, J. Louvet, B.L. Smith, A. Zucchini. Theoretical experimental study of flexible roof effects in an HCDA's simulation. *Proc. 8th Int. Conf. on Structural Mechanics In Reactor Technology*, Paper E 4/5, 139–144, Brussels, Belgium, August 1985.

[21] J.L. Graveleau, P. Louvet. Calculation of fluid-structure interaction for reactor safety with the CASSIOPEE code. *Proc. 5th Int. Conf. on Structural Mechanics In Reactor Technology*, Paper B 1/7, Berlin, Germany, August 1979.

[22] A. Hoffmann, M. Lepareux, B. Schwab, H. Bung. Plexus – A general computer program for fast dynamic analysis. *Proc. Conference on Structural Analysis and Design on Nuclear Power Plant*, Porto Alegre, Brazil, 1984.

[23] H. Holtbecker. Testing philosophy and simulation techniques. *Nuclear Engineering and Design* **42**: 75–87, 1977.

[24] N.E. Hoskin, M.J. Lancefield. The COVA programme for the validation of computer codes for fast reactor containment studies. *Nuclear Engineering and Design*, **46**: 17–46, 1978.

[25] I.E. Idel'Cik. *Memento des pertes de charge. Coefficients de pertes de charge singuličres et de pertes de charge par frottement.* Collection de la Direction des Etudes et Recherche d'EDF, Eyrolles, Paris, France: 362–365, 1986.

[26] K.C. Kendall, A. Benuzzi. The COVA programme: Validation of the fast reactor containment code SEURBNUK. *Nuclear Engineering and Design*, **57**: 79–105, 1980.

[27] K.C. Kendall, D.J. Adnams. *Experiments to validate structural dynamics code used in fast reactor safety assessment.* Science and Technology of Fast Reactor Safety, Vol. 2, British Nuclear Energy Society, London, England, 1986.

[28] M. Lepareux, B. Schwab, A. Hoffmann, P. Jamet, H. Bung. Un programme général pour l'analyse dynamique rapide – Cas des tuyauteries. *Proc. Colloque Tendances Actuelles en Calcul des Structures*, Bastia, France, 1985.

[29] M. Lepareux, B. Schwab, H. Bung. Plexus: A general computer program for the fast dynamic analysis. The case of pipe-circuits. *Proc. 8th Int. Conf. on Structural Mechanics In Reactor Technology*, Paper F1 2/1, Brussels, Belgium, 1985.

[30] M. Lepareux, H. Bung, A. Combescure, J. Aguilar. Analysis of a CDA in a LMFBR with a multiphasic and multicomponent behaviour law. *Proc. 11th Int. Conf. on Structural Mechanics In Reactor Technology*, Paper E 13/1, 371–376, Tokyo, Japan, August 1991.

[31] M. Lepareux, H. Bung, A. Combescure, J. Aguilar, J.F. Flobert. Analysis of an HCDA in a fast reactor with a multiphase and multicomponent behavior law. *Proc. 12th Int. Conf. on Structural Mechanics In Reactor Technology*, Paper E 7/2, 197–202, Stuttgart, Germany, August 1993.

[32] M. Lepareux, J.M. Michelin, D. Thiault. Plexus-R : une extension de Plexus à la robotique. CEA report DMT/94–138, 1994.

[33] J. Louvet, P. Hamon, B.L. Smith, A. Zucchini. MARA 10: an integral model experiment in support of LMFBR containment analysis. *Proc. 9th Int. Conf. on Structural Mechanics In Reactor Technology*, Vol. E: 331-337, Lausanne, Switzerland, August 1987.

[34] J. Louvet. Containment response to a core energy release. Main experimental and theorical issues - Future trends. *Proc. 10th Int. Conf. on Structural Mechanics In Reactor Technology*, Vol. E: 305-310, Anaheim, USA, August 1989.

[35] NERSA. *The Creys-Malville power plant, Electricité de France.* Direction de l'équipement, Région d'équipement Alpes-Lyon, France, 1987.

[36] M.F. Robbe, M. Lepareux, H. Bung. Plexus – Notice théorique. CEA report DMT/94–490, 1994.

[37] M.F. Robbe, P. Galon, T. Yuritzinn. Castem-Plexus: Un logiciel de dynamique rapide pour évaluer l'intégrité des structures en cas d'accident. *Proc. 4th Conf. INSTRUC*, Courbevoie, France, November 1999.

[38] M.F. Robbe, Y. Cariou, M. Lepareux, E. Treille. Computation of the MARS test simulating a Hypothetical Core Disruptive Accident in a small scale replica of a Fast Breeder Reactor. *Proc. Int. Conf. on Numerical Methods in Continuum Mechanics 2000*, CD-rom, Liptovsky Jan, Slovak Republic, September 2000.

[39] M.F. Robbe, Y. Cariou, E. Treille, M. Lepareux. Comparison of a Core Disruptive Accident simulation with the MARS experimental test. *Proc. Int. Conf. on Numerical Methods in Continuum Mechanics 2000*, CD-rom, Liptovsky Jan, Slovak Republic, September 2000.

[40] M.F. Robbe, N. Vivien, M. Valette, E. Berglas. Use of thermalhydraulic and mechanical linked computations to estimate the mechanical consequences of a steam explosion. *Journal of Mechanical Engineering*, **52** (2): 65–90, 2001.

[41] M.F. Robbe, M. Lepareux, E. Treille, Y. Cariou. Numerical simulation of an explosion in a simple scale model of a nuclear reactor. *Journal of Computer Assisted Mechanics and Engineering Sciences*, **9** (4): 489–517, 2002.

[42] M.F. Robbe, M. Lepareux. Evaluation of the mechanical consequences of a steam explosion in a nuclear reactor. *Bulgarian Journal of Theoretical and Applied Mechanics*, **32** (1): 48–84, 2002.

[43] M.F. Robbe, M. Lepareux, C. Trollat. Hydrodynamic loads on a PWR primary circuit due to a LOCA. *Nuclear Engineering and Design*, **211**: 189-228, 2002.

[44] M.F. Robbe, F. Bliard. A porosity method to describe the influence of internal structures on a fluid flow in case of fast dynamics problems. *Nuclear Engineering and Design*, **215**: 217–242, 2002.

[45] M.F. Robbe, M. Lepareux, Y. Cariou. Numerical interpretation of the MARA 8 experiment simulating a Hypothetical Core Disruptive Accident. *Nuclear Engineering and Design*, **220**: 119–158, 2003.

[46] M.F. Robbe, M. Lepareux, E. Treille, Y. Cariou. Numerical simulation of a Hypothetical Core Disruptive Accident in a simple scale model of a nuclear reactor. *Nuclear Engineering and Design*, **223**, (2): 159–196, 2003.

[47] M.F. Robbe, M. Lepareux. Comparison of the numerical results of Europlexus with the MARS experiment. *Proc. 11th Int. Conf. On Nuclear Engineering*, CD-rom, Tokyo, Japon, Paper 403, April 2003.

[48] M.F. Robbe, P. Sardain. Comparison of several simplified models and scenarios to simulate a steam explosion in a tank. *Journal of Mechanical Engineering*, **54** (2): 82–100, 2003.

[49] M.F. Robbe, S. Potapov, F. Teffany. Simulation of the depressurisation occuring at the beginning of a LOCA in a 4-loop PWR. *Nuclear Engineering and Design*, **223**: 159–196, 2003.

[50] M.F. Robbe, S. Potapov. Modeling of the depressurisation induced by a pipe-rupture in the primary circuit of a nuclear plant. *Revue Européenne des Eléments Finis* **12** (4): 459–485, 2003.

[51] M.F. Robbe, F. Casadei. Comparison of various models for the simulation of a Core Disruptive Accident in the MARA 10 mock-up. *Nuclear Engineering and Design*, **232**: 301–326, 2004.

[52] M.F. Robbe, M. Lepareux, E. Seinturié. Results of the simulation of a Core Disruptive Accident in the MARS mock-up. *Proc. 4th Student Conf. of the American Nuclear Society*, CD-rom, Madison University, Winsconsin, USA, April 2004.

[53] J.E.A. Sidoli, K.C. Kendall. The WINCON programme – Validation of the fast reactor primary containment codes. *Proc. INE Int. Conf. On Nuclear Containment*, Cambridge, England, April 1987. Nuclear Containment Structures, D.G. Walton, Cambridge University Press, 1988.

[54] B.L. Smith, A. Yerkess, J. Adamson. Status of coupled fluid-structure dynamics code SEURBNUK. *Proc. 7th Int. Conf. on Structural Mechanics In Reactor Technology*, Paper B 9/1, Chicago, USA, August 1983.

[55] B.L. Smith, C. Fiche, J. Louvet, A. Zucchini. A code comparison exercise based on the LMFBR containment experiment MARA-04. *Proc. 8th Int. Conf. on Structural Mechanics In Reactor Technology*, Paper E 4/7, 151–157, Brussels, Belgium, August 1985.

[56] B.L. Smith, A. Yerkess, V. Washby. The computer code SEURBNUK-EURDYN: First release version. *Proc. 9th Int. Conf. on Structural Mechanics In Reactor Technology*, Lausanne, Switzerland, August 1987.

[57] M. Stiévenart, P. Bouffioux, M. Eglème, J.P. Fabry, H. Lamotte. Analysis of LMFBR explosion model experiments by means of the Surboum-II code. *Proc. 3rd Int. Conf. on Structural Mechanics In Reactor Technology*, Paper E 3/5, London, England, August 1975.

[58] E. Studer, P. Galon. Hydrogen combustion loads – Plexus calculations. *Nuclear Engineering and Design*, **174**: 119–134, 1997.

[59] H.U. Wenger, B.L. Smith. On the origin of the discrepancies between theory and experiment in the COVA series. *Proc. 9th Int. Conf. on Structural Mechanics In Reactor Technology*, Vol. E: 339-344, Lausanne, Switzerland, 1987.

[60] P.H. West, N.E. Hoskin. APRICOT – Phase 3. Suggested simple test problems for examination of thin shell modelling and fluid structure coupling. Aldermaston report AWRE/44/92/16, 1980.